

<i>IASF- Sez. di Bologna</i>	<b>SCIENTIFIC PERFORMANCE REPORT</b>	<i>Ref:R P Issue: 1 Date: 03/02/04 page: 1/41</i>
--------------------------------------	--------------------------------------	---

***Spectroscopic characterization of two CdZnTe Multipixel Detectors  
in an eV Multi Pix 16 Channel ASIC Evaluation System***

N. Auricchio, J. B. Stephen, E. Caroli, A. Donati, G. Landini,  
F. Schiavone, G. Ventura, F. Frontera, A. Basili, T. Franceschini

Istituto di Astrofisica Spaziale e Fisica Cosmica  
Sezione di Bologna

Internal Report n. 387

<i>IASF- Sez. di Bologna</i>	<b>SCIENTIFIC PERFORMANCE REPORT</b>	<i>Ref: R P Issue: 1 Date: 03/02/04 page: 2/41</i>
--------------------------------------	--------------------------------------	--

## **TABLE OF CONTENTS**

- Summary
- 1. Introduction
- 2. Experimental set-up
- 3. CdZnTe Detector Calibration
  - 3.1 Analysis of the spectra
  - 3.2 Signal to noise ratio at different gain values
  - 3.3 Shaping time at different gain values
  - 3.4 Pixel Spectra
  - 3.5 Gain and offset derivation method
    - 3.5.1 Gain 200
    - 3.5.2 Gain 50
- 4. Detector performance evaluation
  - 4.1 Pulse amplitude
  - 4.2. Energy Resolution
  - 4.3. Peak to valley ratio
  - 4.4. Relative Detection Efficiency
  - 4.5 Energy threshold
  - 4.6. Stability of P51134 detector
- 5. Conclusions
- Annex 1 Measurement Logbook
- Annex 2 Fitting models

<b>IASF-</b> <b>Sez. di</b> <b>Bologna</b>	<b>SCIENTIFIC PERFORMANCE REPORT</b>	<i>Ref: R P</i> <i>Issue: 1</i> <i>Date: 03/02/04</i> <i>page: 3/41</i>
--	--------------------------------------	--

## ***Summary***

In this report we present the results of a detailed spectroscopic characterization study of two CdZnTe multipixel detectors included in an eV Multi Pix 16 channel ASIC Evaluation System. The measurements have been carried out using a standard electronic chain. The purpose of this study is to investigate the spectral performances of every pixel and the uniformity of the detectors.

### ***1. Introduction***

#### ***Why CdTe and CdZnTe detectors?***

Semiconductor detectors have long been used as gamma-ray and x-ray spectrometers. The materials that provide the best efficiency and energy resolution require cryogenic cooling for their operation. This places considerable constraints on the application of these materials for space environments. In the last few years several semiconductor materials have emerged that allow room temperature operation. Unfortunately the technology for producing these crystals is not yet mature and they still have significant shortcomings such as poor carrier transport properties and non-uniformity. These parameters limit both the maximum active volume that can be utilized, which constrains the radiation absorption efficiency, and the energy resolution achievable.

Cadmium Zinc Telluride (CdZnTe) is one of the most promising of the room temperature semiconductor detectors for gamma-ray detection. The high-density ( $5.8 \text{ g cm}^{-3}$ ) and the high atomic number of the materials (48,30, 52 ) give a high detection efficiency for gamma rays. Moreover CZT has a high resistivity and low leakage current which is favorable for low noise applications. However, incomplete charge collection due to poor charge transport properties of these materials degrades the energy resolution and lowers the effective photopeak efficiency for gamma rays. The properties of CdTe and CZT semiconductor materials are reported in following table in comparison with those of traditional materials:

**Table 1.** The properties of semiconductor materials.

	<b>Si</b>	<b>Ge</b>	<b>CdZnTe</b>	<b>CdTe</b>
Atomic Number Z	14	32	<b>48 - 30 - 52</b>	48 - 52
Density ( $\text{g} \cdot \text{cm}^{-3}$ )	2.33	5.32 (77 K)	<b><math>\approx 6.0</math></b>	6.06
Bandgap (eV)	1.12	0.74 (77 K)	<b>1.5 - 2.2</b>	1.47
Energy for electron/hole pair (eV)	3.61	2.98 (77 K)	<b>5.0</b>	4.43
Resistivity ( $\Omega \cdot \text{cm}$ )	$2.3 \cdot 10^5$	47	<b><math>10^{11}</math></b>	$2 \div 3 \cdot 10^9$
$(\mu\tau)_e$ ( $\text{cm}^2 \cdot \text{V}^{-1}$ )	4.5	3.9	<b><math>1 \cdot 10^{-3}</math></b>	$10^{-3}$
$(\mu\tau)_h$ ( $\text{cm}^2 \cdot \text{V}^{-1}$ )	1.8	1.8	<b><math>6 \cdot 10^{-6}</math></b>	$0.8 \cdot 10^{-4}$

#### ***Why CdTe and CdZnTe detectors for Hard X-ray and gamma ray astrophysics?***

CZT is a room temperature operating semiconductor well suited for high energy X-ray astronomy: this detector is ideal for both X-ray all-sky survey missions as well as focal plane detectors in X-ray focusing optics missions. We are studying the application of position sensitive detectors made of this material for polarization measurements in hard X- and soft  $\gamma$ -ray astronomy. A recent result from the RHESSI solar observatory suggests that, at least in gamma-ray bursts, high energy emission may be strongly polarised. In July 2002 the POLCA (POLarimetry with Cadmium telluride Array) experiment was tested at the European Synchrotron Research Facility at Grenoble, France, where monochromatic beams (almost 100% linearly polarised) at 100, 300 and 400 keV have been utilised to irradiate CdTe arrays containing elements of thickness between 3 and 8 mm. The next step concerns the irradiation, with a complete energy coverage over the 100-1000 keV

range, of a CdZnTe matrix composed of 4 pixellated detectors, in order to increase the active area and allow a study of polarisation efficiency (Q-factor) against detector dimensions. Each detector contains 16 elements (4x4), that are 5 mm in thickness. Two of these detectors have been calibrated and the results reported here.

## 2. Experimental set-up

This technical note describes the work performed at IASF/CNR – Sezione Bologna in the period 2003 December-2004 January on an eV Multi Pix 16 channel ASIC Evaluation System.

The eV Multi Pix 16 channel ASIC Evaluation System is designed to give the user a platform to evaluate the eV Products' 16 channel ASIC paired with a 4x4 channel CdZnTe detector at room temperature. This system is capable of sensing X-rays or gamma rays in the energy range of 10 keV to 1.5 MeV. The thickness of the detector included with this device is 5 mm, while the lateral dimensions are 10.6x10.6 mm<sup>2</sup>, the pixel size is 1.8 x 1.8 mm<sup>2</sup> (2 mm pitch) +0.5 guard ring.

The ASIC in this unit accepts an input from either the CdZnTe detector or an external pulser and produces one unipolar shaped signal for each photon detected or pulse injected. The ASIC channel outputs have ~ 300 mV of DC offset and the operating voltage is 3.0 V. The detector bias voltage is 520 V.

Other features of the unit include:

- An on-board adjustable High Voltage Bias Supply.
- A 100:1 Voltage Divided High Voltage Monitor BNC Connector.
- DIP Switch control of ASIC gain and peaking time.
- Ability to operate from a single +12 V power supply.
- Test pulse connection through a BNC Connector.
- DIP Switch control of the channel connected to the test input injection capacitor.
- BNC connectors for CZT Channel Outputs.
- 20-pin ribbon cable connector for access to all 16 ASIC channel outputs.

### Adjustable High Voltage Power Supply

The eV Multi Pix 16 channel ASIC Evaluation System is equipped with an on board High Voltage Power Supply that is capable of biasing the CZT detector from -330 V to -600 V (adjust the potentiometer as shown in Fig. 1.). The voltage is fixed at 512 V.

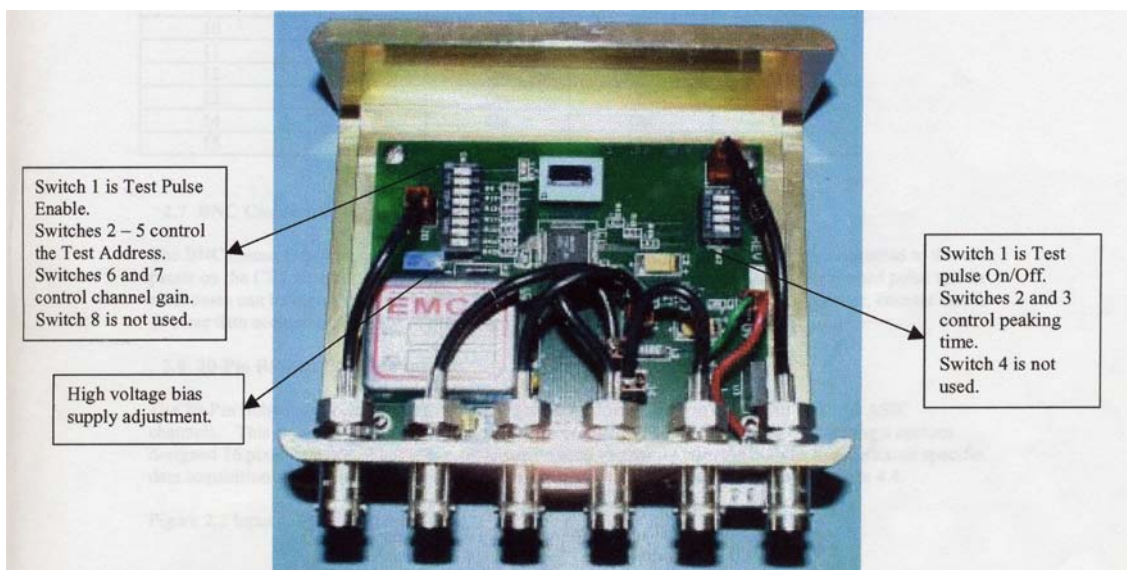


**Fig.1.** The box containing the pixellated CZT matrix: control switches and bias supply adjustment.

**HV monitor**

The HV monitor connection point provides a 1000:1 reduction in the actual High Voltage Power Supply output voltage level so a measurement of -0.45 V at the BNC corresponds to a bias level of -450 V.

**Power Supply Connection**

The eV Multi Pix 16 Channel ASIC Evaluation System requires a +12 V power supply unit.

**Test pulse input Enable**

The test pulse input can be attached to the BNC connector as shown in Fig. 2. This input is then routed through a DIP switch as shown in Fig. 1.

If this switch is in the ON position the test pulse is fed to the on chip 100 fF test pulse injection capacitor. In the OFF position the test pulse is not routed to the ASIC therefore no output pulse will be seen.

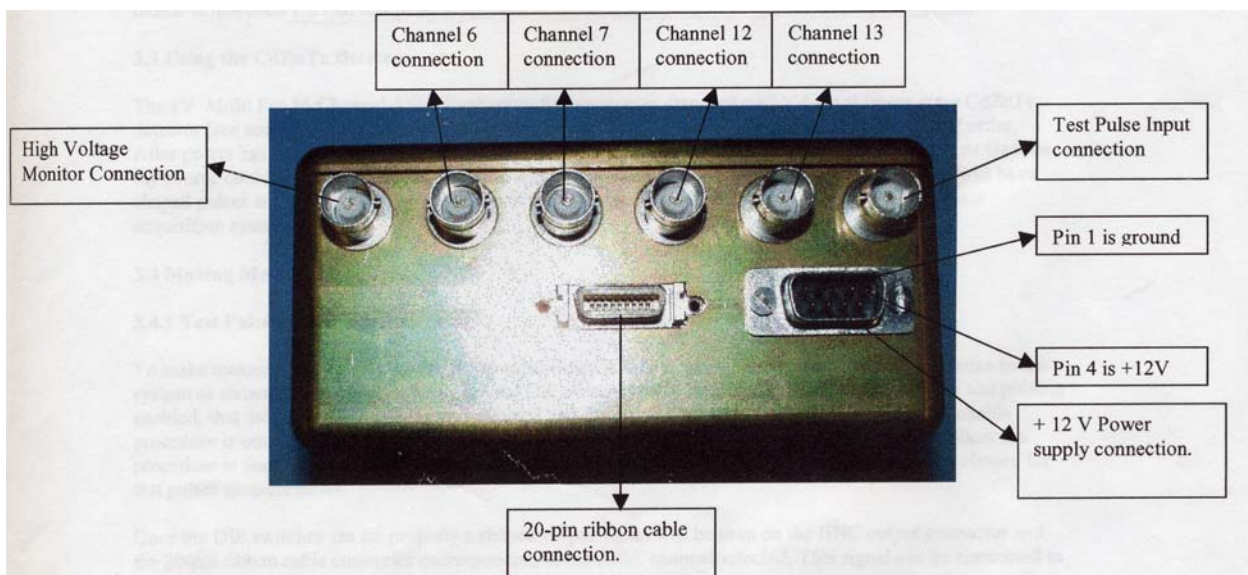


Fig. 2. Input and output connections.

**Test channel address Control**

The test channel address control is found on the DIP switch (see Fig. 1). This switch determines which ASIC channel receives the test pulse input signal from the external BNC connection.

**BNC connectors for CZT Outputs**

The BNC connectors shown in Fig. 2 allow access to the 4 ASIC channels that are connected to the 4 pixels on the CZT detector. The signal on these connectors will be a positive unipolar shaped pulse that can be directly connected to a MCA, ADC, counter board or other data acquisition system. These outputs can drive a load of 1 Kohm || 200 pF.

**20-Pin ribbon cable connector**

The 20-Pin ribbon cable connector shown in Fig. 2. allows access to the output of all 16 ASIC channels. This is useful when testing a custom designed 16 pixel detector. The ribbon cable can be used to directly wire the outputs to a customer specific data acquisition system.

**ASIC gain and peaking time**

The 16 channel ASIC is capable of amplifying an input signal by 4 gain values: 200, 100, 50, 33. These are controlled by internal DIP switches as shown in Fig. 3.

<b>IASF-</b> <b>Sez. di</b> <b>Bologna</b>	<b>SCIENTIFIC PERFORMANCE REPORT</b>	<i>Ref: R P</i> <i>Issue: 1</i> <i>Date: 03/02/04</i> <i>page: 6/41</i>
--	--------------------------------------	--

The ASIC provides 4 different peaking time values in order to shape the input signal: 0.6, 1.2, 2.4, 4.0  $\mu$ s. These are controlled by internal DIP switches as shown in Fig. 3.

The peaking time is correlated with the shaping time by following relation:

$$\text{Peaking time} = n \times \tau$$

where:

$\tau$  = Shaping time

n = number of stages of integration.

The schematic drawing of the control switches is illustrated in Fig. 3 and their position is reported in table 2 and 3:

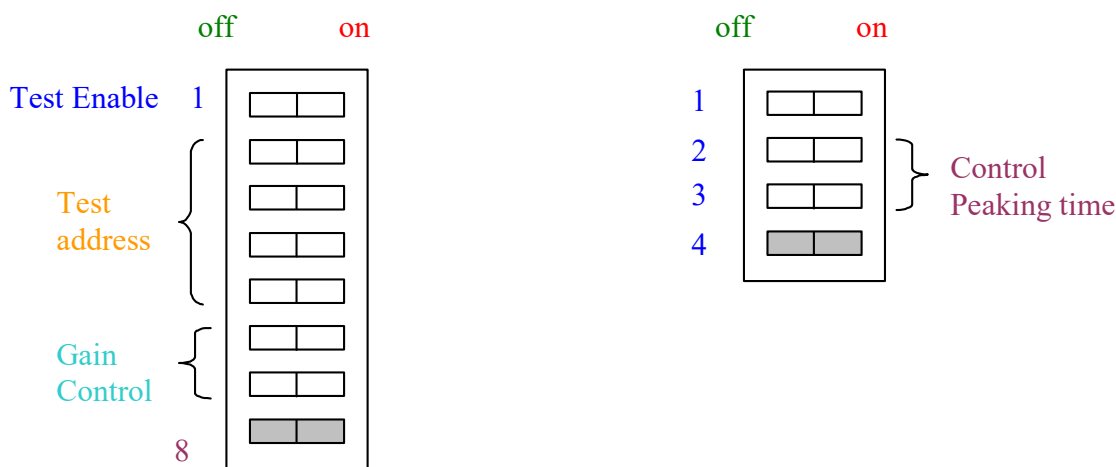


**Fig. 3.** Control switches.

**Table 2.** Switch Position for gain control.

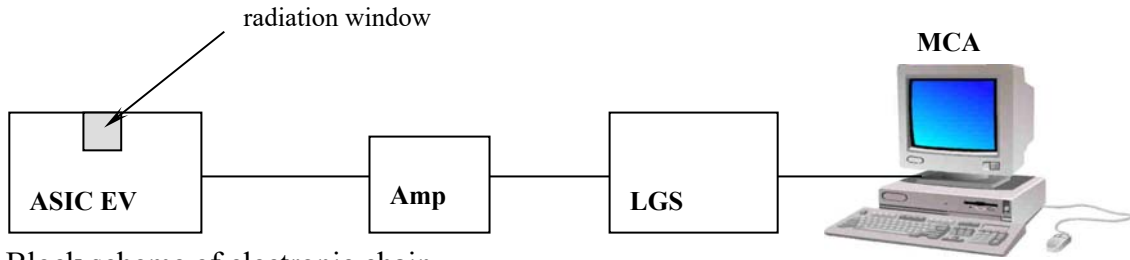
Gain (mV/fC)	Switch 6	Switch 7
200	Off	Off
100	On	Off
50	Off	On
33	On	On

**Table 3.** Switch Position for Peaking Time control.

Peaking Time ( $\mu$ s)	Switch 2	Switch 3
0.6	Off	Off
1.2	On	Off
2.4	Off	On
4.0	On	On

A schematic diagram of the experimental configuration employed for testing the multipixel detector is sketched in Fig. 4. The modules used are:

- eV Multi Pix 16 channel **ASIC Evaluation System**;
- AC coupled Linear **Amplifier** home made to eliminate the DC offset and to amplify the voltage level of  $\sim 4$  times;
- Ortec **Linear Gate and Stretcher mod. 542**;
- **MCA Aptec 3000**.

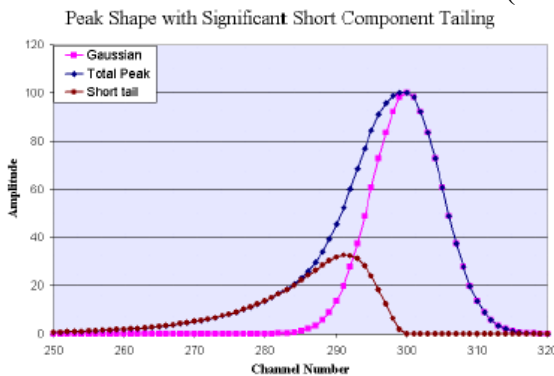
**Fig. 4.** Block scheme of electronic chain.

### 3. CdZnTe Detector Calibration

To make measurements using CZT detector all test pulser capabilities were disabled . This provides the lowest noise measurement and therefore the best results. The measurements were performed at various gains and with different uncollimated radioactive sources ( $^{241}\text{Am}$ ,  $^{57}\text{Co}$ ,  $^{137}\text{Cs}$ ), placed over the radiation window. The ASIC output shaped pulses were connected from every pixel to the AC coupled linear amplifier and applied to an MCA (see Fig. 4), via LGS. The aim of these measurements is to evaluate for every pixel the gains and offsets of the pulse-height, the energy resolution, the charge collection efficiency (centroid position), the peak to valley ratio and finally the uniformity. Some measurements have been performed with collimated  $^{57}\text{Co}$  and  $^{137}\text{Cs}$  beams ( $\phi = 3.5$  mm and 5 mm) to evaluate the possibility of carrying out collimated measurements but we have used only the  $^{57}\text{Co}$  measurements collimated with  $\phi = 5$  mm in order to evaluate the optimal shaping time value for different gains. The detectors tested are labelled with the serial numbers **698300**/revision c and **P51134**.

#### 3.1 Analysis of the spectra

The spectra have been analysed using the PeakFit software package (PeakFit v4.0. Peak separation and Analysis Software: User's Manual, Jandel Scientific Software, 1995) in order to obtain several parameters (e.g. efficiency, photopeak pulse amplitude, energy resolution). The main characteristics of the spectra are: a Gaussian photopeak component corresponding to the energy of the incident photons and an asymmetric component caused by trapping effects. The first component has been modelled using a Gaussian distribution and the second was fitted using a typical chromatographic asymmetric function known as a Half-Gaussian Modified Gaussian (see Annex 2).



#### 3.2 Signal to noise ratio at different gain values

Table 4 reports the measured signal to noise ratio. By definition noise is any fluctuation that appears superimposed on a signal source. There are several sources of fluctuations in a measuring system and they affect the energy resolution with broadening of the full energy photopeak:

$$FWHM_{TOT} = \sqrt{FWHM_{statistical}^2 + FWHM_{electronic}^2 + \dots}$$

IASF- Sez. di Bologna	<b>SCIENTIFIC PERFORMANCE REPORT</b>	Ref: R P Issue: 1 Date: 03/02/04 page: 8/41
-----------------------------	--------------------------------------	--

It is worth noticing that 200 is the gain that gives the best signal to noise ratio, as shown in table.

**Table 4.** Signal to noise ratio.

Gain ASIC	Signal at 60 keV (mV)	Noise (mV)	Signal/Noise
33	60	10	<b>6.0</b>
50	84	12	<b>7.0</b>
100	170	15 ÷ 20	<b>11.3 ÷ 8.5</b>
<b>200</b>	<b>340</b>	<b>20 ÷ 30</b>	<b>13.0 ÷ 17.0</b>

### 3.3 Shaping time at different gain values

A set of measurements has been carried out, irradiating detector **698300** with a  $^{57}\text{Co}$  source, at gains of 50, 100, 200 and varying the shaping time from 0.6  $\mu\text{s}$  to 2.4  $\mu\text{s}$  to evaluate the optimum value for each gain. The output signal of some pixels, that were selected as having lower energy resolution values, have been connected to an MCA. Two basic indicators of the spectra quality, the centroid position and the FWHM, have been derived, and the centroid variation and the energy resolution have been calculated (Table 5). The centroid variation is defined in this way:

$$\Delta\% C = (C_x - C_{\max})/C_{\max} \times 100\% \quad \text{where } C_{\max} = \text{overall centroid maximum value.}$$

This parameter takes the charge collection efficiency changes into consideration. The choice of the optimal peaking time value depend on trade-off considerations: first of all the energy resolution should be the best achievable, secondly the charge collection efficiency loss should be minimized.

**Table 5.**  $\Delta\% C$  and energy resolution for different peaking time values.

Gain 50						
	Peaking Time = 0.6 $\mu\text{s}$		Peaking Time = 1.2 $\mu\text{s}$		Peaking Time = 2.4 $\mu\text{s}$	
Pixel	$\Delta\% C$	Energy Resolution (%)	$\Delta\% C$	Energy Resolution (%)	$\Delta\% C$	Energy Resolution (%)
2	-18.94	11.54	-5.33	8.86	-3.62	9.64
6	-16.08	10.65	-3.59	9.16	-3.67	9.78
11	-14.03	9.88	-0.90	9.36	0.00	9.49
15	-17.09	10.96	-4.19	9.90	-3.69	10.35
Gain 100						
	Peaking Time = 0.6 $\mu\text{s}$		Peaking Time = 1.2 $\mu\text{s}$		Peaking Time = 2.4 $\mu\text{s}$	
Pixel	$\Delta\% C$	Energy Resolution (%)	$\Delta\% C$	Energy Resolution (%)	$\Delta\% C$	Energy Resolution (%)
2	-10.54	4.71	-3.24	4.42	-1.57	4.70
6	-10.88	4.40	-3.79	4.26	-3.23	4.41
11	-9.36	4.37	-1.43	4.07	0.00	4.24
15	-11.01	4.76	-3.21	4.23	-1.93	4.71
Gain 200						
	Peaking Time = 0.6 $\mu\text{s}$		Peaking Time = 1.2 $\mu\text{s}$		Peaking Time = 2.4 $\mu\text{s}$	
Pixel	$\Delta\% C$	Energy Resolution (%)	$\Delta\% C$	Energy Resolution (%)	$\Delta\% C$	Energy Resolution (%)
2	-7.36	4.74	-3.30	3.31	-2.05	3.52
6	-8.07	4.55	-2.85	3.14	-0.94	3.20
11	-7.33	4.64	-1.81	3.22	-0.16	3.29
15	-7.70	4.18	-2.30	3.69	0.00	3.56

It is noticeable that the better peaking time value is 12  $\mu\text{s}$  for all the gain value.

### 3.4 Pixel Spectra

The spectra of all pixels are shown in the following figures when they are irradiated with several radioactive sources ( $^{57}\text{Co}$ ,  $^{241}\text{Am}$ ,  $^{137}\text{Cs}$ ).

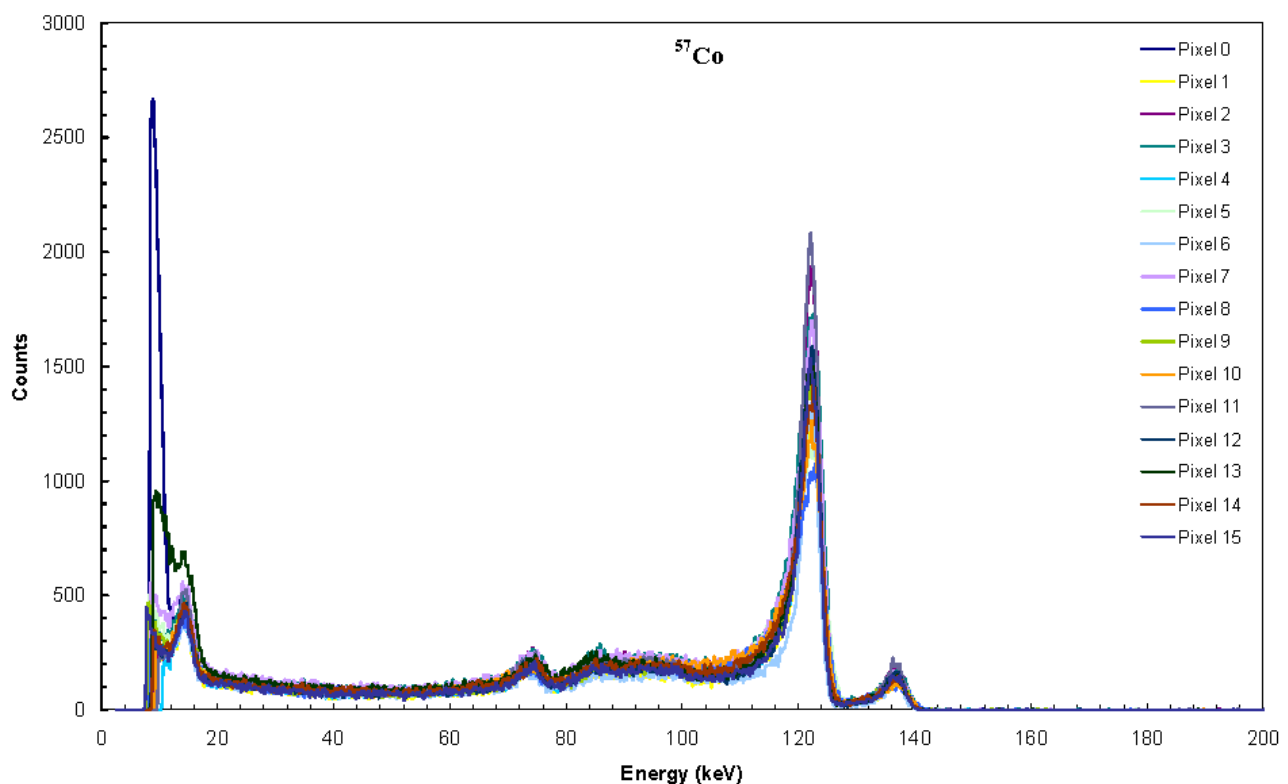
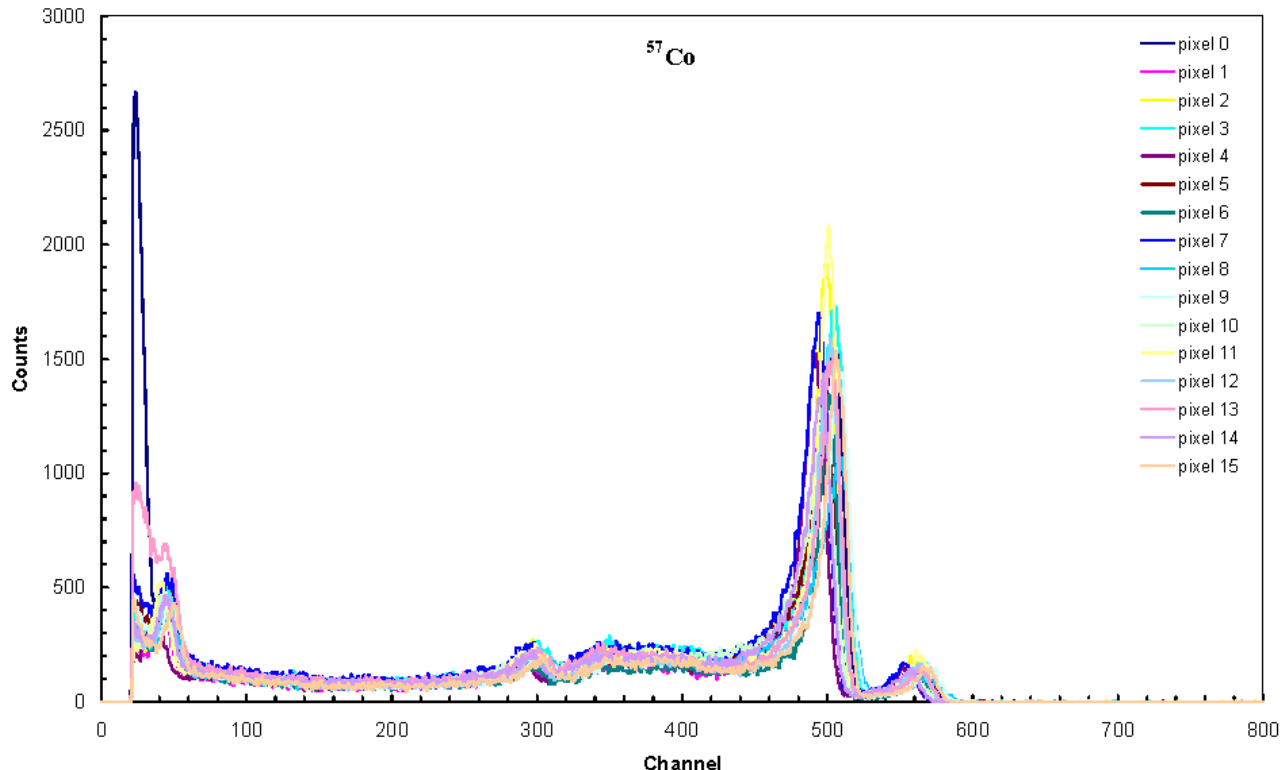


**Fig. 5.**  $^{57}\text{Co}$  spectra of detector **698300** pixels both before and after energy calibration.

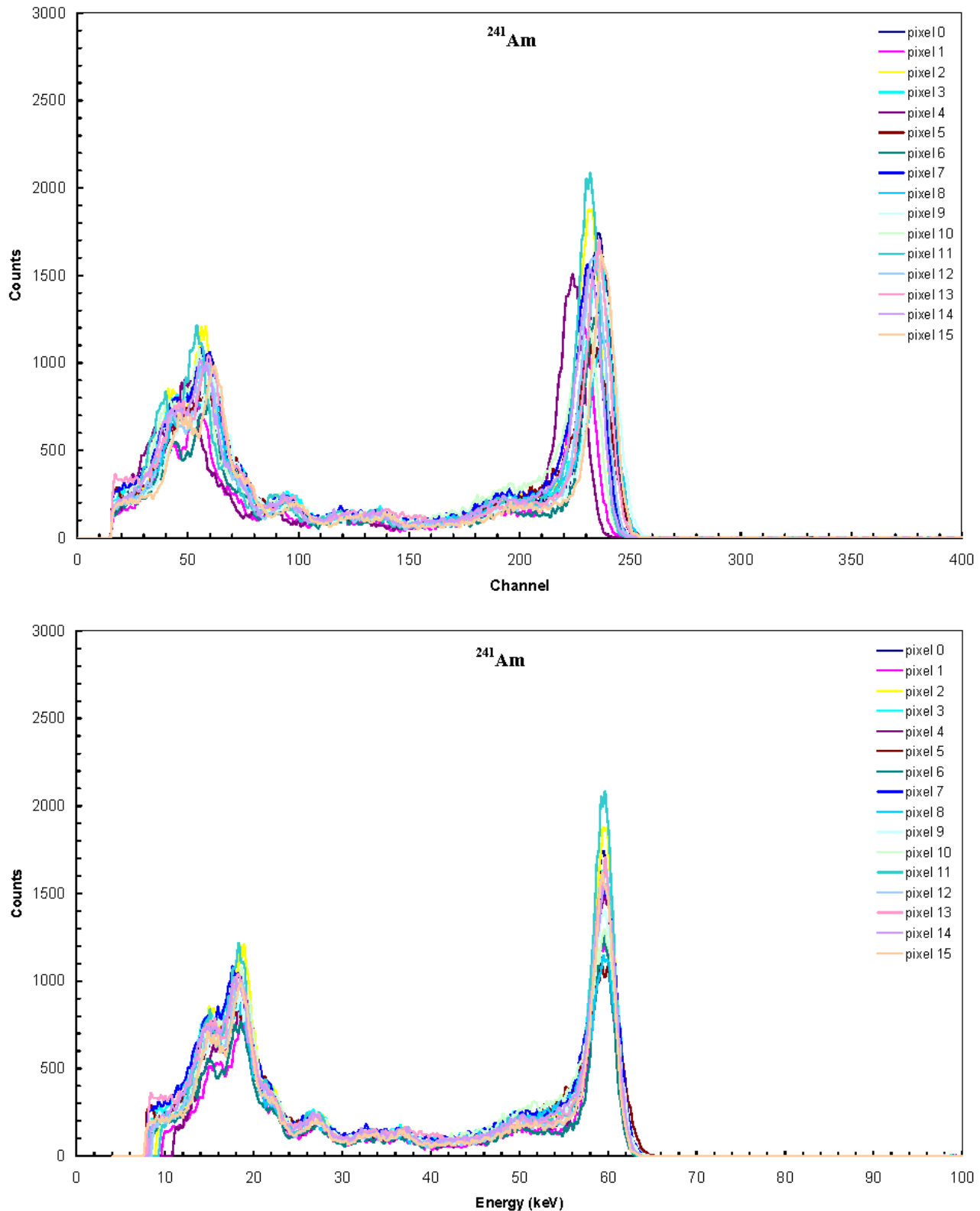


**Fig. 6.**  $^{241}\text{Am}$  spectra of detector 698300 pixels both before and after energy calibration.

The amplifier gain used in measurements plotted until now is 200, because at this value the signal to noise ratio is better, while that employed in order to obtain the spectra by the  $^{137}\text{Cs}$  source is 50, because at 100 and 200 the spectrum is out of range.

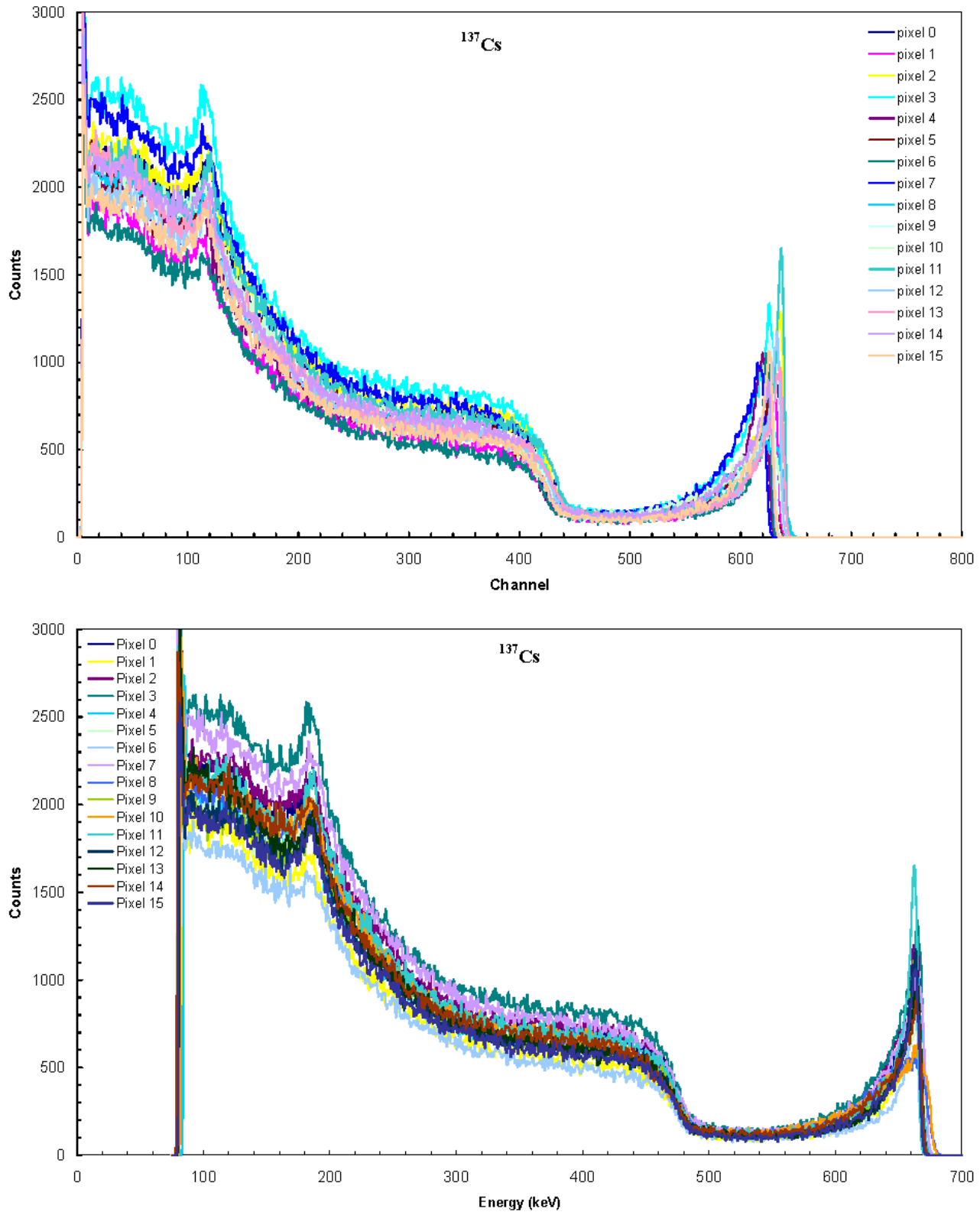


**Fig. 7.**  $^{137}\text{Cs}$  spectra of detector 698300 pixels both before and after energy calibration.

The spectra of each pixel are shown in following figures when they are irradiated with several radioactive sources ( $^{57}\text{Co}$ ,  $^{241}\text{Am}$ ,  $^{137}\text{Cs}$ ). The same considerations are effective about the gain value.

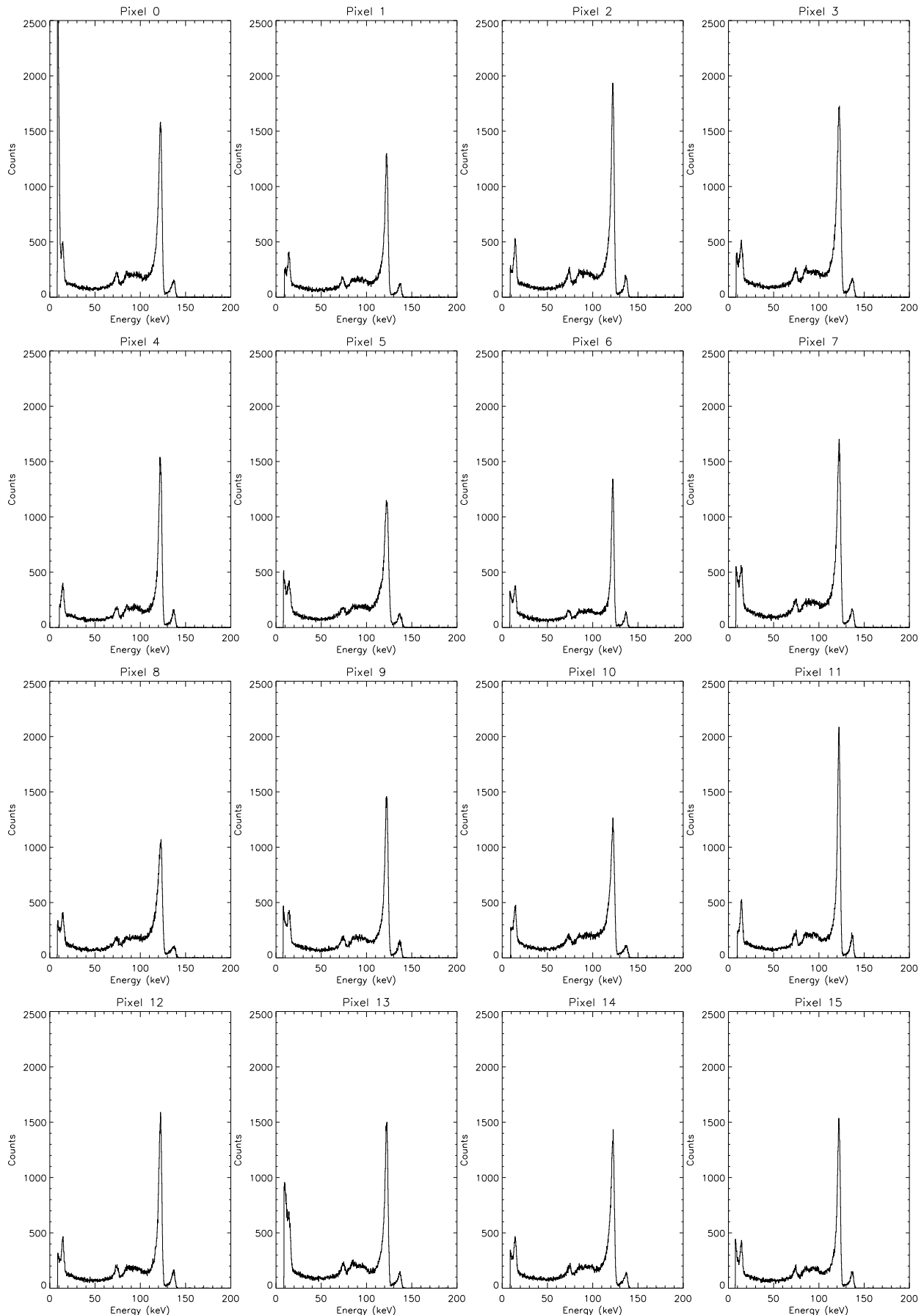


**Fig. 8a.**  $^{57}\text{Co}$  spectra of detector 698300 pixels after energy calibration.

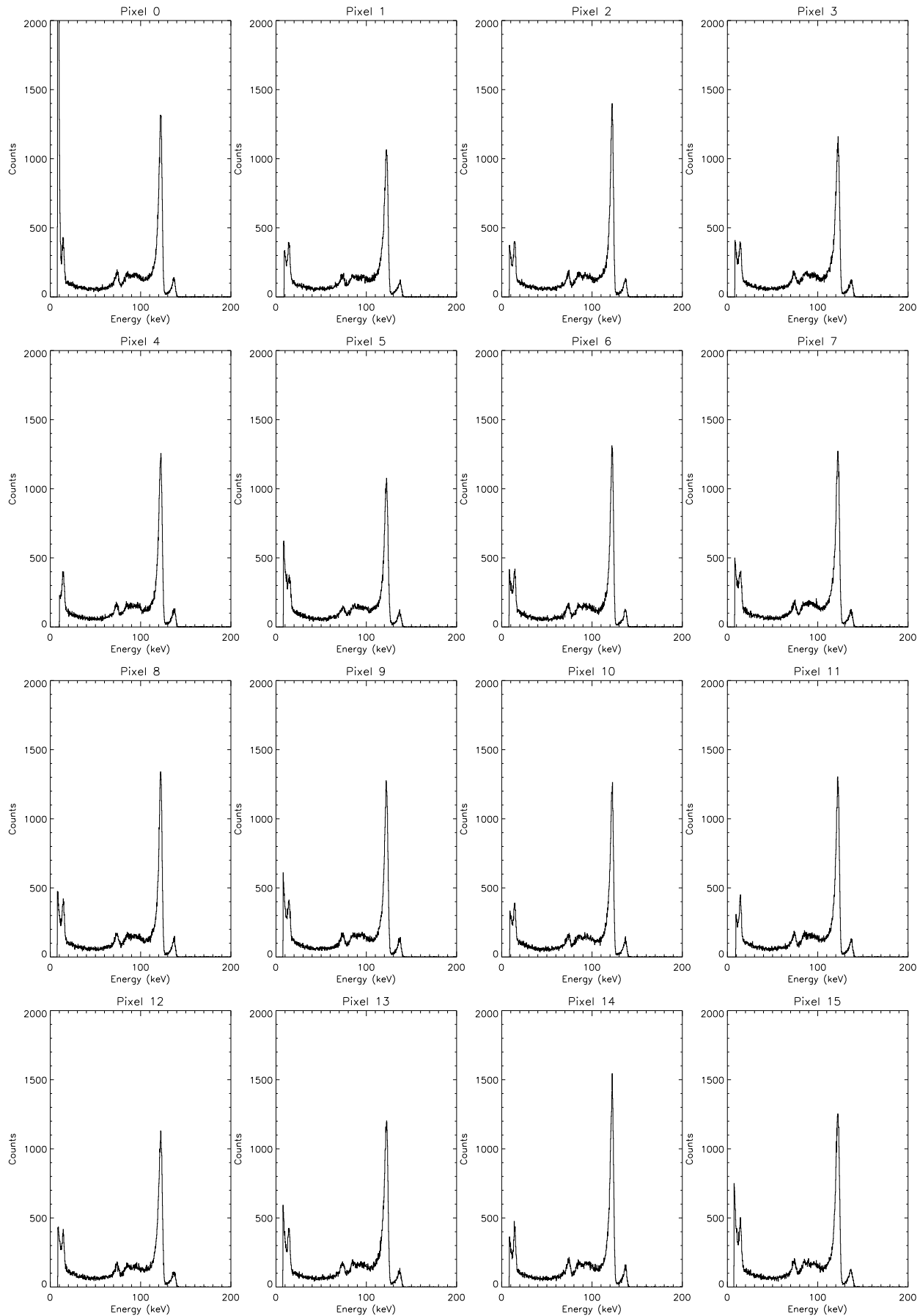


**Fig. 8b.**  $^{57}\text{Co}$  spectra of detector P51134 pixels after energy calibration.

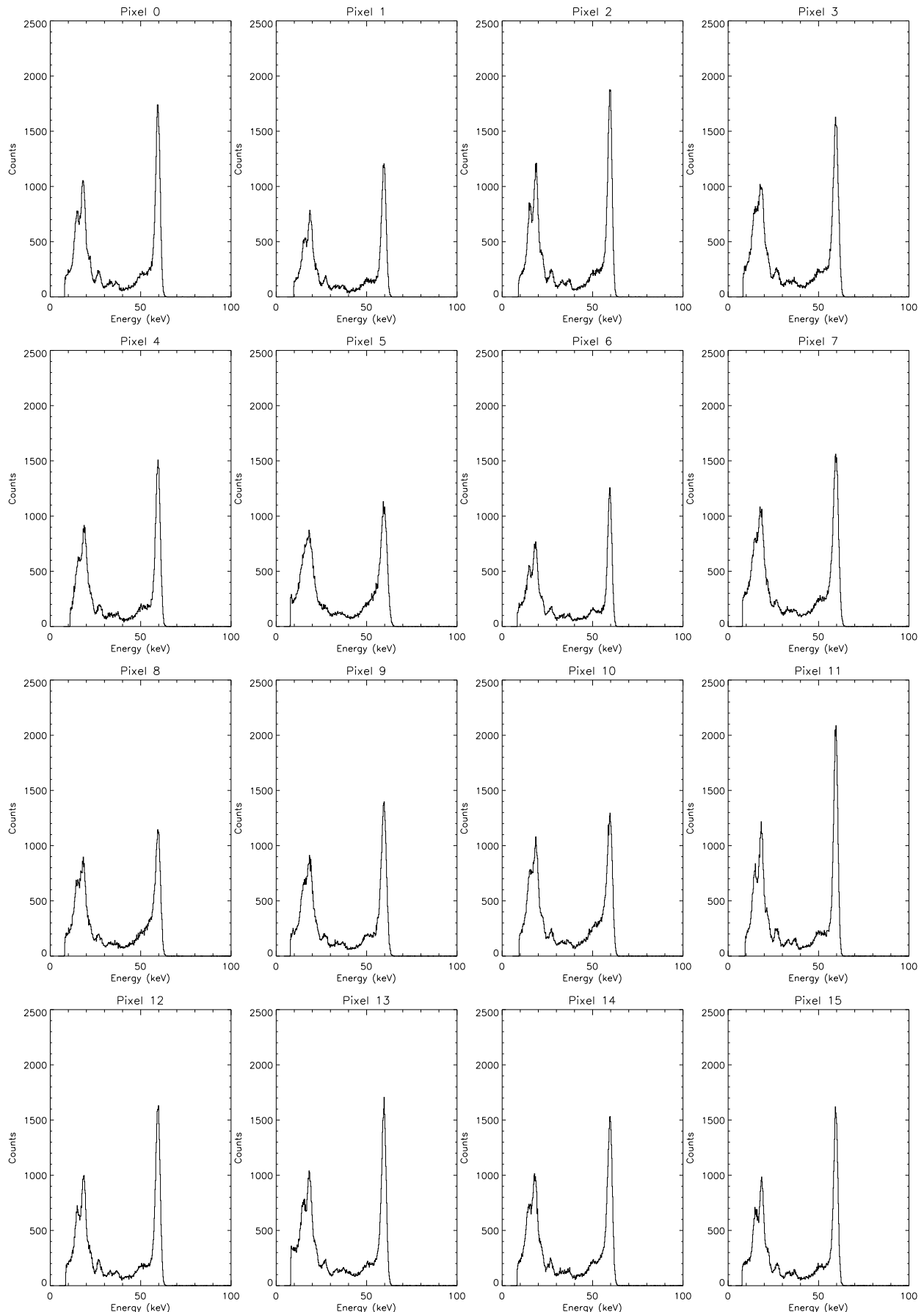


**Fig. 9a.**  $^{241}\text{Am}$  spectra of detector **698300** pixels after energy calibration.

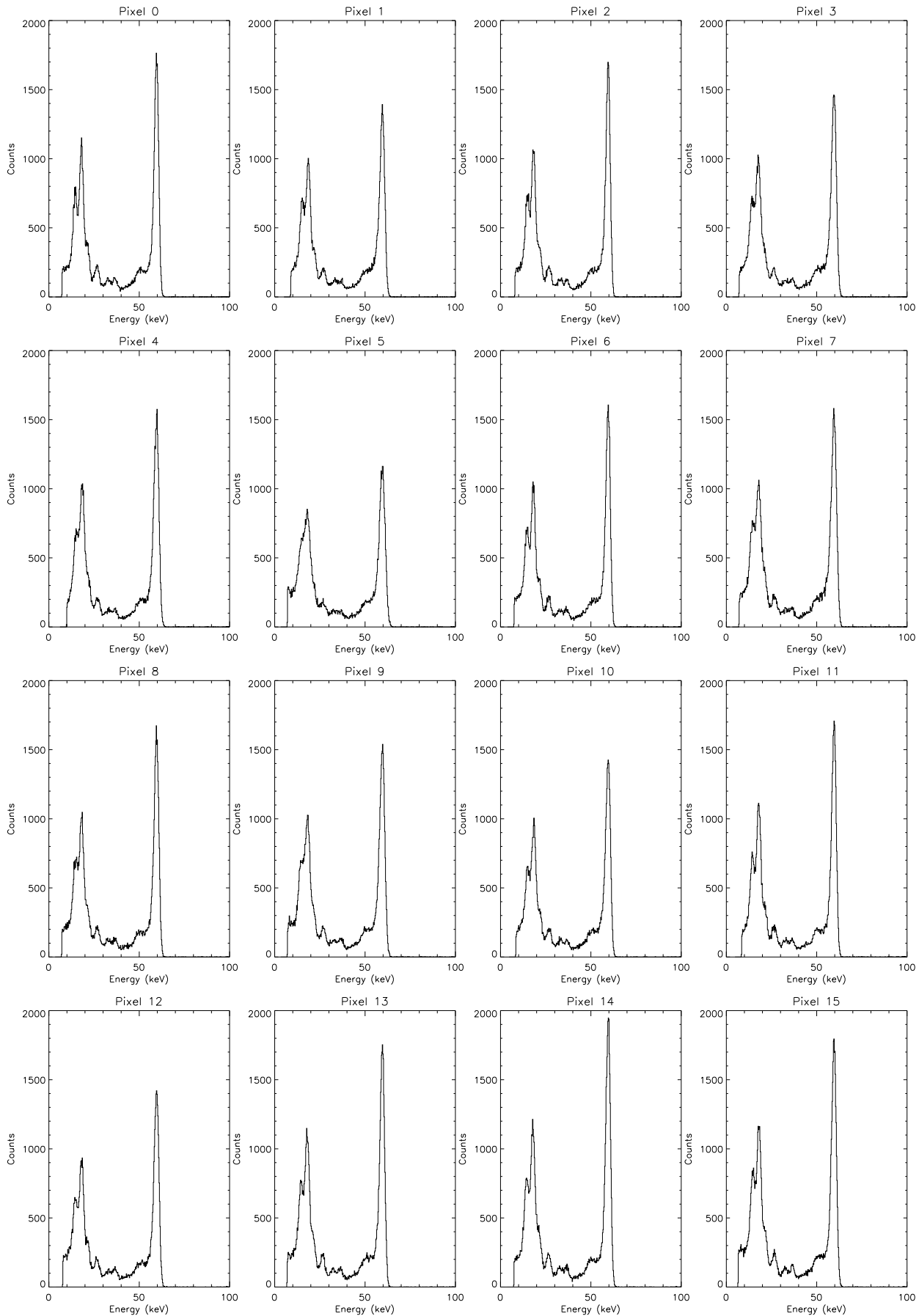


**Fig. 9b.**  $^{241}\text{Am}$  spectra of detector **P51134** pixels after energy calibration.

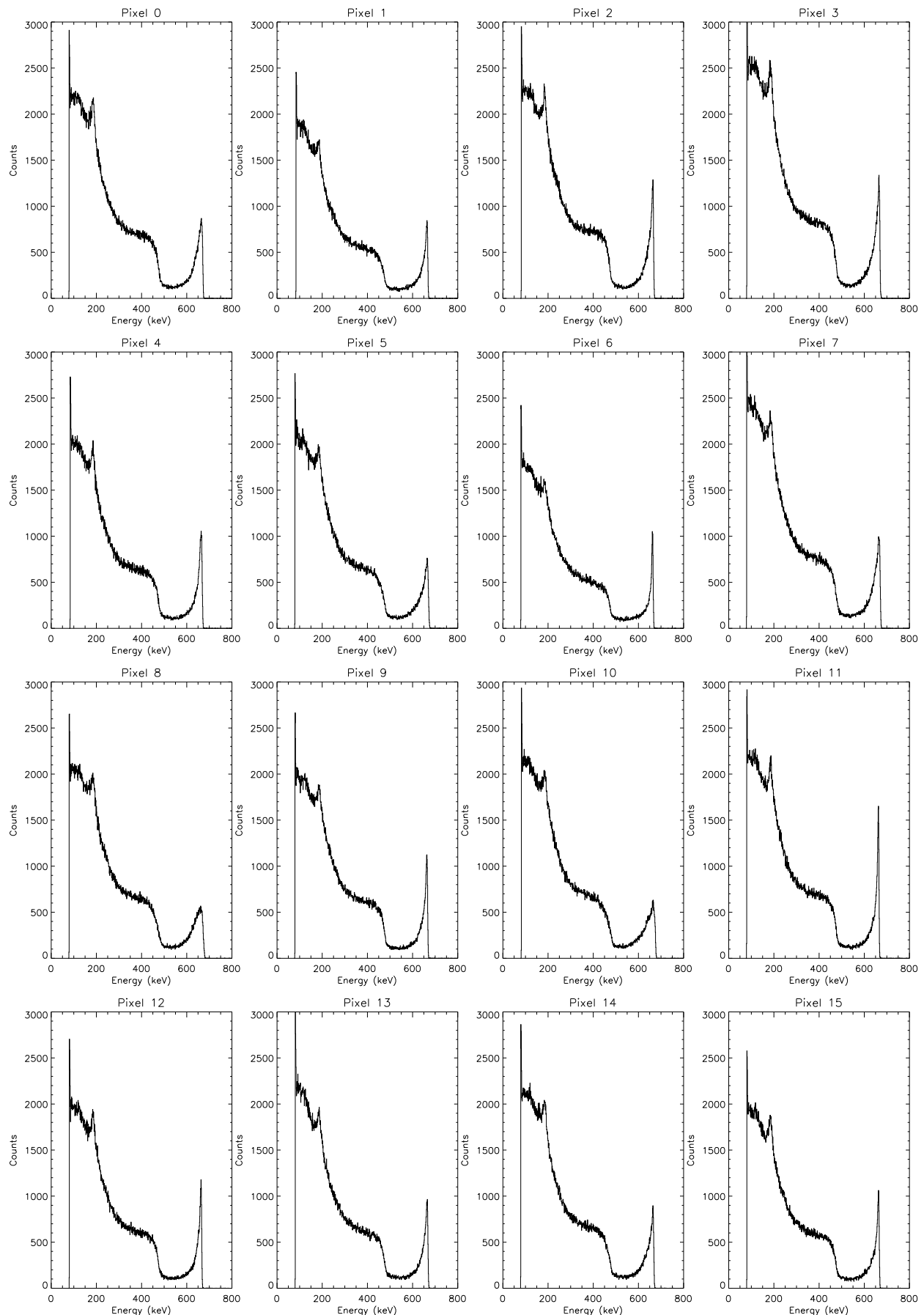


**Fig. 10.**  $^{137}\text{Cs}$  spectra of detector 698300 pixels after energy calibration.

<b>IASF- Sez. di Bologna</b>	<b>SCIENTIFIC PERFORMANCE REPORT</b>	<i>Ref: R P Issue: 1 Date: 03/02/04 page: 17/41</i>
--------------------------------------	--------------------------------------	---

It is possible to note that:

- only two pixels are noisy, 0 and 13 in 698300; 0,5 and 15 in P51134;
- the uniformity of the response of each pixel, as defined by the distribution of the full energy peak centroid channel and of the relative photopeak efficiency is quite homogeneous;
- in the  $^{241}\text{Am}$  spectrum we can observe the lines at  $\sim 13.95$ ,  $17.75$  and  $26.34$  keV;
- in the  $^{57}\text{Co}$  spectrum we can observe the characteristic X rays at  $\sim 72$  and  $75$  keV of the Pb cover;
- in the  $^{137}\text{Cs}$  spectrum we can observe the backscatter peak at  $\sim 186$  keV in accordance with the theoretical value of  $184.32$  keV.

### 3.5 Gain and offset derivation method

#### 3.5.1 Gain 200

The technique usually used to derive the gain and the offset for each pixel requires measurements with good statistics ( $\sim 5 \cdot 10^4$  counts per pixel) and at least two lines well separated in the spectrum. For high-energy lines, the peak efficiency is low and the first of the above requirements implies very strong sources or very long measurements. Neither of these conditions is desirable. The  $^{57}\text{Co}$  source provides a satisfactory compromise with 108 keV between two lines (14.41 and 122.06 keV) and an efficiency close to 95% for the 122 keV line. In the following table a coarse determination of the pulse height obtained using **Aptec** software is reported together with energy resolution values which are typical for this type of detector. The centroid values at 14 and 122 keV have been used to energy calibrate the  $^{57}\text{Co}$  spectrum and thereby evaluate the gain and offset. In the last column of table 6 we have reported the offset expressed in channels:

$$\text{offset(channel)} = \frac{-\text{offset(keV)}}{\text{gain}}$$

**Table 6a.** Centroid, energy resolution @ 14 and 122 keV; offset and gain values for 698300.

Pixel	Centroid at 14 keV (channel)	Energy Resolution at 14 keV (%)	Centroid at 122 keV (channel)	Energy Resolution at 122 keV (%)	Gain (keV/ch)	Offset (keV)	Offset (channel)
0	47.12	15.78	503.07	3.68	0.236	3.29	-13.93
1	43.07	19.83	495.44	3.20	0.238	4.16	-17.50
2	45.03	24.77	498.44	3.29	0.237	3.72	-15.68
3	46.43	27.52	503.62	4.15	0.235	3.48	-14.78
4	37.80	27.36	491.32	3.51	0.237	5.44	-22.92
5	47.46	23.04	496.61	4.45	0.240	3.04	-12.68
6	46.51	19.66	500.49	2.81	0.237	3.39	-14.28
7	46.68	22.08	492.72	3.71	0.241	3.15	-13.04
8	47.37	23.70	506.36	4.48	0.235	3.30	-14.09
9	49.16	24.53	507.41	3.52	0.235	2.86	-12.19
10	42.92	23.77	495.89	3.93	0.238	4.21	-17.73
11	41.29	24.28	500.56	2.81	0.234	4.74	-20.20
12	45.94	21.65	500.76	3.36	0.237	3.54	-14.95
13	45.17		501.93	3.31	0.236	3.77	-15.99
14	44.86	24.67	494.63	3.50	0.239	3.68	-15.36
15	49.96	19.99	506.16	3.14	0.236	2.63	-11.13

The average of these values is: gain = **0.237** keV/channel, offset = **3.65** keV.

The average of the offset value expressed in channel is: offset = - **15.40** channel.

IASF- Sez. di Bologna	SCIENTIFIC PERFORMANCE REPORT	Ref: R P Issue: 1 Date: 03/02/04 page: 18/41
-----------------------------	-------------------------------	---

The dispersion of the gains and offsets is about 1% and 19 % from the mean value.

**Table 6b.** Centroid, energy resolution @ 14 and 122 keV; offset and gain values for P51134.

Pixel	Centroid at 14 keV (channel)	Energy Resolution at 14 keV (%)	Centroid at 122 keV (channel)	Energy Resolution at 122 keV (%)	Gain (keV/ch)	Offset (keV)	Offset (channel)
0	48.41	14.59	498.04	3.52	0.239	2.82	-11.80
1	43.52	21.22	485.34	4.01	0.244	3.81	-15.63
2	46.03	21.39	490.13	3.31	0.242	3.26	-13.43
3	46.98	20.40	494.76	4.32	0.240	3.12	-12.97
4	38.98	27.34	483.20	3.75	0.242	4.97	-20.49
5	46.69		484.52	3.76	0.246	2.93	-11.93
6	47.03	21.33	491.31	3.38	0.242	3.02	-12.46
7	47.14	21.67	484.12	4.02	0.246	2.80	-11.36
8	49.04	21.41	497.49	3.28	0.240	2.64	-11.01
9	48.65	18.25	494.47	3.69	0.241	2.67	-11.04
10	43.88	19.17	485.45	3.38	0.244	3.72	-15.24
11	42.86	22.73	493.67	3.74	0.239	4.18	-17.50
12	46.23	15.32	488.16	3.92	0.244	3.15	-12.94
13	49.46	21.87	499.10	3.81	0.239	2.57	-10.75
14	46.04	16.41	485.86	3.38	0.245	3.14	-12.84
15	51.03	18.86	498.05	4.05	0.241	2.12	-8.82

The average of these values is: gain = **0.242** keV/channel, offset = **3.18** keV. The average of the offset value expressed in channel is: offset = - **13.14** channel. The dispersion of the gains and offsets is about 1% and 22 % from the mean value.

In following tables a coarse determination of the pulse height at 59.54 keV, obtained using Aptec software, is reported together with energy resolution values at 59.54 keV, which are typical for this type of detector. The centroid values at 59.54 and 122 keV have been used to energy calibrate the <sup>241</sup>Am spectrum and therefore evaluate the gain and offset.

**Table 7a.** Centroid position, energy resolution @ 59.54 keV; offset and gain values for 698300.

Pixel	Centroid at 59.54 keV (channel)	Energy Resolution at 59.54 keV (%)	Gain (keV/channel)	Offset (keV)	Offset (channel)
0	235.99	5.36	0.234	4.30	-18.35
1	228.50	5.54	0.234	6.02	-25.71
2	231.43	5.20	0.234	5.35	-22.86
3	235.60	6.00	0.233	4.58	-19.65
4	223.65	5.91	0.234	7.30	-31.26
5	233.84	7.52	0.237	4.18	-17.60
6	231.26	5.02	0.234	4.71	-20.11
7	237.37	5.90	0.239	4.24	-17.74
8	238.14	6.24	0.232	4.37	-18.79
9	238.14	5.97	0.232	4.25	-18.29
10	229.43	6.55	0.235	5.71	-24.34
11	231.41	4.89	0.232	5.78	-24.90
12	233.54	5.41	0.234	4.90	-20.94
13	235.25	5.12	0.234	4.39	-18.71
14	231.37	5.96	0.237	4.59	-19.33
15	237.92	4.93	0.233	4.09	-17.53

<b>IASF- Sez. di Bologna</b>	<b>SCIENTIFIC PERFORMANCE REPORT</b>	<i>Ref: R P Issue: 1 Date: 03/02/04 page: 19/41</i>
--------------------------------------	--------------------------------------	---

The average of these values is:

gain = **0.234** keV/channel

offset = **4.92** keV

offset = **-21.01** channel

The dispersion of the gains and offsets is about 1% and 18 % from the mean value.

**Table 7b.** Centroid position, energy resolution @ 59.54 keV; offset and gain values for P51134.

Pixel	Centroid at 59.54 keV (channel)	Energy Resolution at 59.54 keV (%)	Gain (keV/channel)	Offset (keV)	Offset (channel)
0	235.22	5.10	0.238	3.586	-15.07
1	225.83	5.75	0.241	5.136	-21.32
2	230.07	4.91	0.240	4.231	-17.60
3	234.10	5.66	0.240	3.390	-14.14
4	222.54	5.95	0.240	6.163	-25.70
5	229.49	6.35	0.245	3.282	-13.39
6	231.60	5.01	0.241	3.786	-15.73
7	229.33	6.17	0.245	3.266	-13.31
8	235.24	5.18	0.238	3.461	-14.52
9	234.08	5.88	0.240	3.336	-13.89
10	226.72	5.64	0.242	4.755	-19.68
11	230.47	4.23	0.238	4.793	-20.18
12	229.70	5.81	0.242	3.979	-16.45
13	236.55	5.30	0.238	3.213	-13.49
14	229.29	5.39	0.244	3.665	-15.04
15	236.83	5.46	0.239	2.856	-11.93

The average of these values is:

gain = **0.241** keV/channel

offset = **3.93** keV

offset = **-16.34** channel

The dispersion of the gains and offsets is about 1% and 22 % from the mean value.

### 3.5.2 Gain 50

In table 8 a coarse determination of the pulse height at 122 keV and 662 keV, obtained using Aptec software, is reported together with energy resolution values at 662 keV, which are typical for this type of detector. The centroid values at 122 and 662 keV have been used to energy calibrate the  $^{137}\text{Cs}$  spectrum and thereby evaluate the gain and offset. The average of these values is:

gain = **0.936** keV/channel

offset = **76.22** keV

offset = **-81.44** channel

The dispersion of the gains and offsets is about 1% and 2 % from the mean value.

The offset value, in this case, is very large because the Linear Gate and Stretcher had a voltage offset, that was eliminated when the gain was increased at 200, therefore the previous measurements are not affected by this Linear Gate and Stretcher offset.

<b>IASF- Sez. di Bologna</b>	<b>SCIENTIFIC PERFORMANCE REPORT</b>	<i>Ref: R P Issue: 1 Date: 03/02/04 page: 20/41</i>
--------------------------------------	--------------------------------------	---

**Table 8.** Centroid position, energy resolution @ 122 and 662 keV; offset and gain values.

Pixel	Centroid at 122 keV (channel)	Centroid at 662 keV (channel)	Energy Resolution at 662 keV (%)	Gain (keV/ch)	Offset (keV)	Offset (channel)
0	50.46	629.67	3.62	0.932	75.05	-80.57
1	45.63	627.78	2.35	0.927	79.77	-86.07
2	48.45	633.00	2.27	0.923	77.34	-83.79
3	49.21	622.40	3.05	0.941	75.74	-80.46
4	44.8	617.52	2.75	0.942	79.85	-84.76
5	50.07	621.31	3.31	0.945	74.77	-79.16
6	49.38	623.04	1.38	0.941	75.61	-80.39
7	49.14	613.18	3.76	0.957	75.05	-78.46
8	50.24	bad	bad	0.936	75.06	-80.24
9	50.31	625.30	1.99	0.938	74.85	-79.76
10	47.41	621.69	4.87	0.940	77.52	-82.50
11	50.66	635.76	1.43	0.922	75.35	-81.71
12	49.45	631.13	1.84	0.928	76.19	-82.14
13	49.23	631.89	2.7	0.926	76.47	-82.58
14	49.97	622.10	2.48	0.943	74.93	-79.46
15	49.13	624.32	1.90	0.938	75.97	-80.99

#### **4. Detector performance evaluation.**

Five parameters must be considered to completely estimate the quality of detector: pulse amplitude corresponding to the photopeak, the energy resolution, the peak to valley ratio, the efficiency and the energy threshold.

##### **4.1 Pulse amplitude**

The pulse amplitude corresponding to the photopeak is directly related to the charge collection efficiency  $\eta(x)$ , function of the depth of interaction. The relationship obtained for a uniform electric field is given by the Hecht equation:

$$\eta(x) = \lambda_e/d [1 - \exp(-(x-d)/\lambda_e)] + \lambda_h/d [1 - \exp(-x/\lambda_h)]$$

where  $d$  is the inter-electrode distance and  $\lambda$  is the  $(\mu\tau V/d)$  value for electrons and holes, that is the mean free path of electrons and holes, when gamma rays are irradiated from the cathode face.

We have calculated the Relative Photopeak Position using PeakFit (see par. 3.1) software and his error as follows:

$$RPP = \frac{C_x - \text{offset}}{C_0 - \text{offset}} = \frac{C_x}{C_0}$$

$$\sigma_{RPP} = \sqrt{\left(\frac{\partial RPP}{\partial C_x} \sigma_{C_x}\right)^2 + \left(\frac{\partial RPP}{\partial C_0} \sigma_{C_0}\right)^2}$$

where:

$C_x$  = photopeak centroid of the pixel  $x$  ( $c_x$ ) - offset;

$C_0$  = photopeak centroid of the pixel 0 ( $c_0$ ) - offset.

$\sigma_{cx}, \sigma_{c0}$  = this error is obtained by fitting procedure;

$\sigma_{Cx}, \sigma_{C0}$  = this error includes the error associated to the offset.

The error associated to the offset has been evaluated as follows:

$$\sigma_{offset} = \left| \frac{offset}{c_x} \right|$$

The behaviour of the relative photopeak position is plotted in Fig. 11.

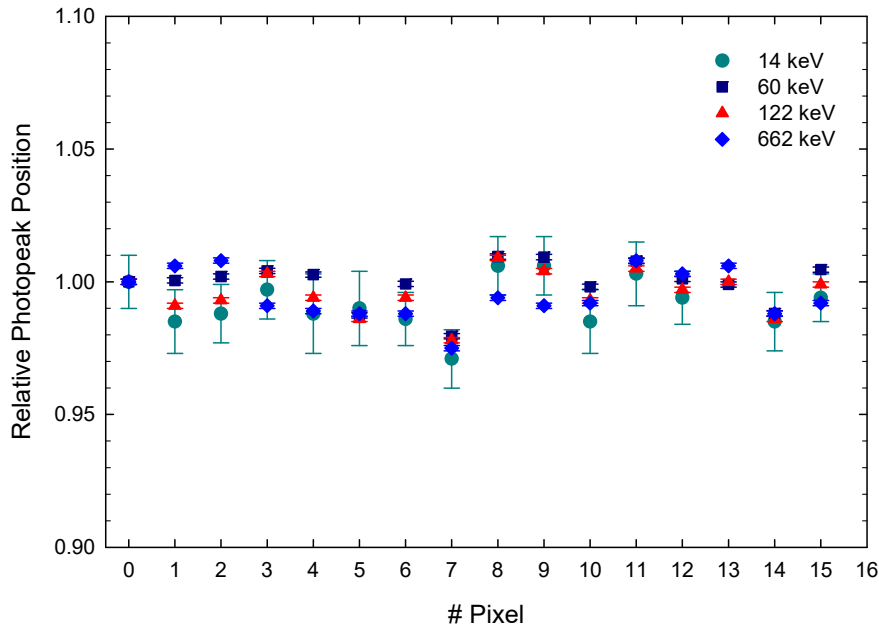


**Fig.11a.** The uniformity of pixel full energy peak centroid for 698300.

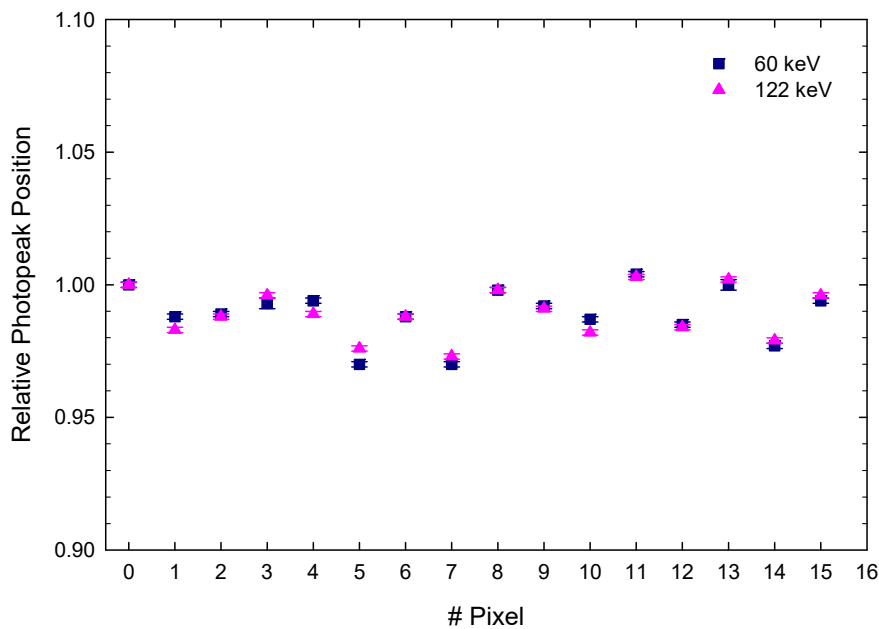


**Fig.11b.** The uniformity of pixel full energy peak centroid for P51134.

It is worth noticing that the uniformity of the relative photopeak position is quite homogeneous: the standard deviation from the mean value is about 1% for both multipixels.

## 4.2 Energy Resolution

In pulse height spectroscopy, the energy resolution of a detector is usually defined as the full width at half maximum (FWHM) of a gamma ray photopeak:

$$\text{Energy Resolution} = \frac{\text{FWHM}}{\text{Centroid} - \text{offset}} \times 100$$

the formula above can be rewritten as:

$$R = \frac{\text{FWHM}}{C} \times 100$$

The error associated to the energy resolution has been evaluated as follows:

$$\sigma_R = \sqrt{\left(\frac{\partial R}{\partial \text{FWHM}} \sigma_{\text{FWHM}}\right)^2 + \left(\frac{\partial R}{\partial C} \sigma_C\right)^2}$$

The same considerations above are effective about the centroid and its error.

The behaviour of the energy resolution is reported in Fig. 12.

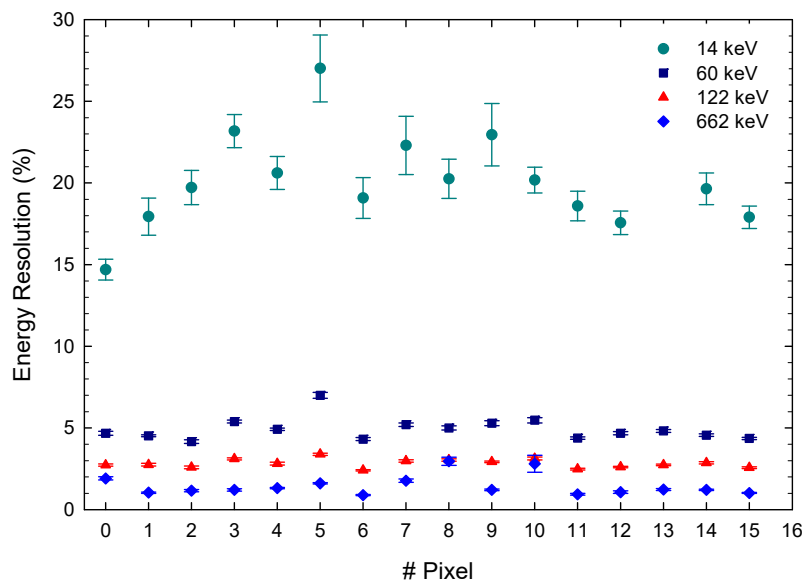


**Fig.12a.** Energy resolution of each pixel at different energies for 698300.

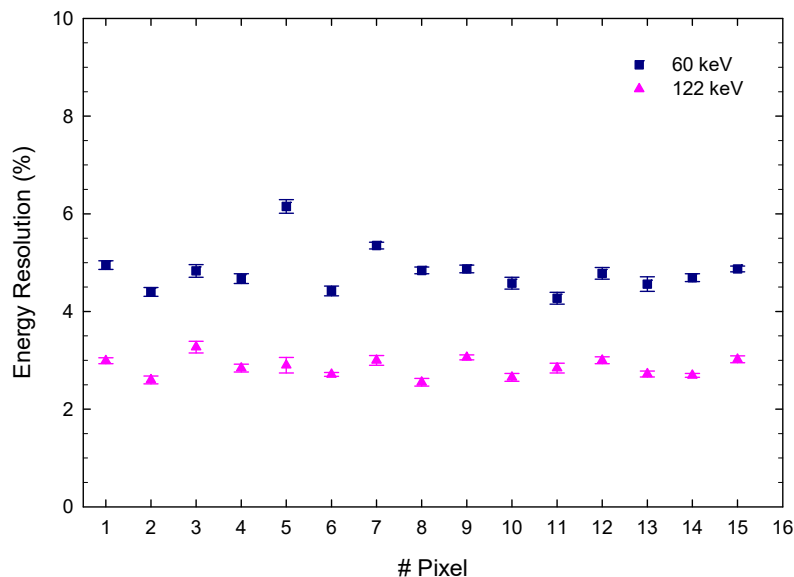


**Fig.12b.** Energy resolution of each pixel at different energies for P51134.

<b>IASF-</b> <b>Sez. di</b> <b>Bologna</b>	<b>SCIENTIFIC PERFORMANCE REPORT</b>	<i>Ref: R P</i> <i>Issue: 1</i> <i>Date: 03/02/04</i> <i>page: 23/41</i>
--	--------------------------------------	---

A summary of values defined above is reported in the following tables for each pixel with the average value.

**Table 9.** FWHM, centroid position and energy resolution at 14 and 122 keV for 698300.

# Pixel	FWHM (keV) at 14 keV	Centroid (channel) at 14 keV	Energy Resolution at 14 keV (%)	FWHM (keV) at 122 keV	Centroid (channel) at 122 keV	Energy Resolution at 122 keV (%)
0	2.12	47.28	14.69	3.34	504.75	2.73
1	2.57	42.79	17.94	3.36	496.31	2.75
2	2.83	44.77	19.72	3.17	499.30	2.59
3	3.33	46.24	23.17	3.81	505.27	3.11
4	2.96	37.55	20.61	3.45	492.46	2.82
5	3.92	47.94	27.01	4.15	498.84	3.39
6	2.73	46.11	19.08	2.94	501.21	2.41
7	3.20	46.37	22.30	3.64	494.16	2.98
8	2.93	47.51	20.25	3.74	509.09	3.04
9	3.32	49.40	22.95	3.58	508.34	2.93
10	2.89	42.55	20.17	3.83	497.44	3.13
11	2.68	41.22	18.59	3.03	501.25	2.48
12	2.53	45.91	17.56	3.19	501.98	2.61
13				3.35	502.90	2.74
14	2.84	44.97	19.64	3.51	495.82	2.87
15	2.57	49.73	17.90	3.14	507.06	2.57
<b>Mean</b>	<b>2.71</b>	<b>45.36</b>	<b>18.85</b>	<b>3.45</b>	<b>501.01</b>	<b>2.82</b>

The spectrum of pixel 13 is too broad for fitting at 14 keV.

**Table 10.** FWHM, centroid position and energy resolution at 59.54 and 662 keV for 698300.

# Pixel	FWHM (keV) at 59.54 keV	Centroid (channel) at 59.54 keV	Energy Resolution at 59.54 keV (%)	FWHM (keV) at 662 keV	Centroid (channel) at 662 keV	Energy Resolution at 662 keV (%)
0	2.79	236.03	4.68	12.69	632.15	1.91
1	2.77	228.81	4.54	6.91	630.67	1.04
2	2.48	232.03	4.16	7.69	634.70	1.16
3	3.21	235.78	5.39	8.03	626.05	1.21
4	2.93	223.80	4.92	8.77	620.23	1.32
5	4.18	233.55	7.00	10.73	624.73	1.61
6	2.58	234.07	4.32	5.90	623.88	0.89
7	3.29	231.42	5.20	11.77	616.43	1.77
8	2.99	237.99	5.00	19.63	628.12	2.96
9	3.15	238.45	5.29	8.05	626.37	1.21
10	3.26	229.56	5.47	18.65	624.71	2.81
11	2.61	231.46	4.38	6.25	636.45	0.94
12	2.79	233.71	4.68	7.07	632.37	1.07
13	2.87	235.41	4.82	8.16	634.59	1.23
14	2.72	232.02	4.56	8.04	624.66	1.21
15	2.60	238.02	4.36	6.77	625.88	1.02
<b>Mean</b>	<b>2.95</b>	<b>233.26</b>	<b>4.92</b>	<b>9.69</b>	<b>627.62</b>	<b>1.46</b>

<b>IASF- Sez. di Bologna</b>	<b>SCIENTIFIC PERFORMANCE REPORT</b>	Ref: R P Issue: 1 Date: 03/02/04 page: 24/41
--------------------------------------	--------------------------------------	---

**Table 11.** FWHM, centroid position and energy resolution at 59.54 and 122 keV for P51134.

# Pixel	FWHM (keV) at 59.54 keV	Centroid (channel) at 59.54 keV	Energy Resolution at 59.54 keV (%)	FWHM (keV) at 122 keV	Centroid (channel) at 122 keV	Energy Resolution at 122 keV (%)
0	2.69	235.46	4.52	3.36	499.20	2.75
1	2.95	226.12	4.95	3.67	486.88	2.99
2	2.62	230.22	4.40	3.18	491.21	2.60
3	2.88	234.57	4.83	4.01	496.20	3.27
4	2.79	223.29	4.67	3.48	484.86	2.84
5	3.66	229.58	6.15	3.55	486.56	2.90
6	2.63	231.79	4.42	3.31	492.33	2.71
7	3.19	229.71	5.35	3.67	485.81	3.00
8	2.88	235.44	4.84	3.12	499.20	2.55
9	2.91	234.60	4.87	3.74	495.58	3.06
10	2.74	227.50	4.58	3.25	486.66	2.65
11	2.55	231.30	4.27	3.48	495.15	2.84
12	2.85	230.37	4.78	3.68	489.75	3.00
13	2.72	236.95	4.56	3.33	501.30	2.72
14	2.80	229.62	4.69	3.30	487.28	2.69
15	2.90	237.18	4.87	3.71	500.08	3.02
<b>Mean</b>	<b>2.86</b>	<b>231.48</b>	<b>4.80</b>	<b>3.49</b>	<b>492.38</b>	<b>2.85</b>

The energy resolution has the same behaviour at 60, 122, 662 keV, whose average value is reported above, while at low energy (14 keV) the curve is different because , being close to the threshold, the errors are very large. The values most deviating from the average have been highlighted.

#### 4.3 Peak to valley ratio

The evaluation of the low-energy tail, due to trapping effects, is important in assessing the quality of the detector. To quantify the tail, the peak-to valley ratio is calculated at several points below the peak. The peak-to-valley ratio is the ratio of the peak counts at the centroid channel, to the channel contents at a point in the spectrum below the peak. The valley is calculated as the average of the 5 channels centred at the following channels: 1) a distance of 2 FWHM from the centroid channel; 2) a distance of 5 FWHM from the centroid channel (see fig. 13). Some quantitative results, concerning this parameter, are reported in table 12a and b for detector 698300.

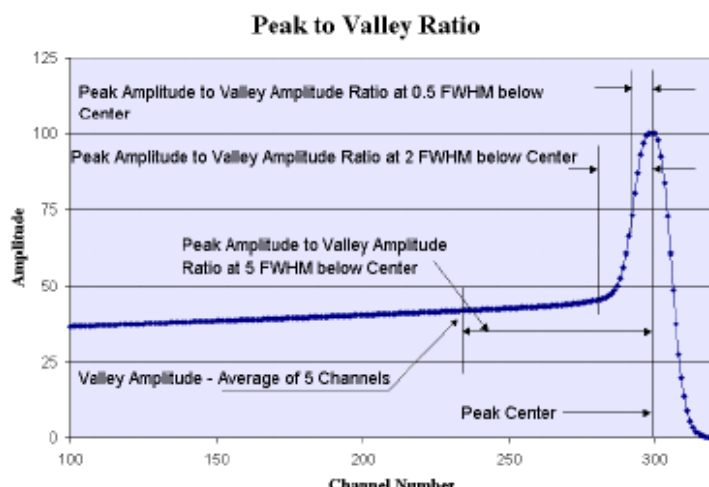


**Fig. 13.** Peak to valley calculation.

<b>IASF-</b> <b>Sez. di</b> <b>Bologna</b>	<b>SCIENTIFIC PERFORMANCE REPORT</b>	<i>Ref: R P</i> <i>Issue: 1</i> <i>Date: 03/02/04</i> <i>page: 25/41</i>
--	--------------------------------------	---

**Table 12a.** Peak to valley ratio at 2 FWHM from the centroid.

# Pixel	Peak to valley ratio at 60 keV	Peak to valley ratio at 122 keV	Peak to valley ratio at 662 keV
0	7.55±0.54	4.11±0.24	1.89±0.11
1	9.59±0.76	4.70±0.32	1.82±0.11
2	7.09±0.48	4.61±0.25	1.90±0.10
3	6.31±0.43	4.56±0.27	1.87±0.10
4	8.16±0.65	5.46±0.36	2.25±0.13
5	5.05±0.38	3.15±0.20	1.80±0.11
6	9.30±0.86	6.18±0.46	2.77±0.17
7	6.00±0.41	4.20±0.24	2.01±0.11
8	4.10±0.28	2.79±0.17	1.68±0.12
9	7.46±0.60	4.99±0.33	2.39±0.13
10	4.14±0.27	3.41±0.21	2.03±0.14
11	9.99±0.73	5.92±0.35	2.56±0.12
12	8.64±0.67	5.00±0.32	2.16±0.12
13	8.18±0.62	4.72±0.030	2.05±0.12
14	5.70±0.39	3.91±0.24	1.77±0.10
15	8.15±0.63	4.94±0.32	2.36±0.13
<b>Mean</b>	<b>7.21</b>	<b>4.54</b>	<b>2.08</b>

**Table 12b.** Peak to valley ratio at 5 FWHM from the centroid.

# Pixel	Peak to valley ratio at 60 keV	Peak to valley ratio at 122 keV	Peak to valley ratio at 662 keV
0	16.28±1.65	8.50±0.68	4.40±0.35
1	15.72±1.57	9.67±0.90	3.37±0.25
2	12.79±1.13	9.93±0.77	3.60±0.22
3	13.35±1.29	8.33±0.63	3.47±0.20
4	16.80±1.87	9.91±0.86	4.66±0.35
5	12.43±1.38	5.82±0.47	3.23±0.25
6	14.86±1.71	10.06±0.93	5.05±0.38
7	13.19±1.29	7.96±0.60	4.25±0.31
8	9.94±1.00	5.78±0.48	4.35±0.43
9	16.13±1.84	9.16±0.78	4.71±0.34
10	11.00±1.09	5.58±0.43	3.95±0.35
11	18.27±1.78	11.75±0.95	4.80±0.29
12	18.44±2.04	10.05±0.87	4.45±0.32
13	15.51±1.57	10.03±0.87	3.86±0.28
14	12.27±1.18	7.88±0.65	2.90±0.19
15	15.65±1.62	10.29±0.91	3.86±0.26
<b>Mean</b>	<b>14.54</b>	<b>8.79</b>	<b>4.06</b>

The data analysis demonstrated that pixels 6 and 11 have a better energy resolution and peak to valley ratio, which is not quite uniform for this detector.

#### 4.4. Detection Relative Efficiency

Another important performance characteristic of radiation detector is the efficiency, which is a measure of its ability to detect the gamma rays. Although the concept of detector efficiency appears

initially to be very simple, in practice there are ambiguities associated with its determination. It is generally defined as the ratio of the counts in the full energy peak and the source emissions. Since there was not a calibrated source at disposal, we have defined the *normalized counts* as the ratio between the total count in each pixel and the mean value of the total counts in the detector. In the same way the *normalized photopeak area* is defined as the ratio between the counts in the full energy peak (area under the photopeak obtained by fitting procedure) in each pixel and the mean value of the photopeak counts in the detector. The area under the photopeak would correspond to the number of measured events in the detector. In the following figure the behaviour of two efficiencies is shown:

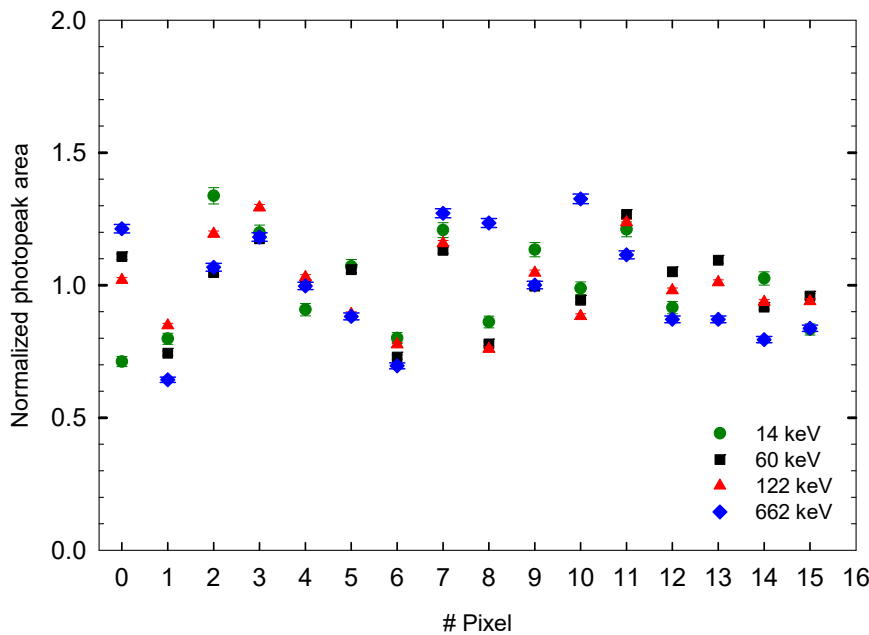
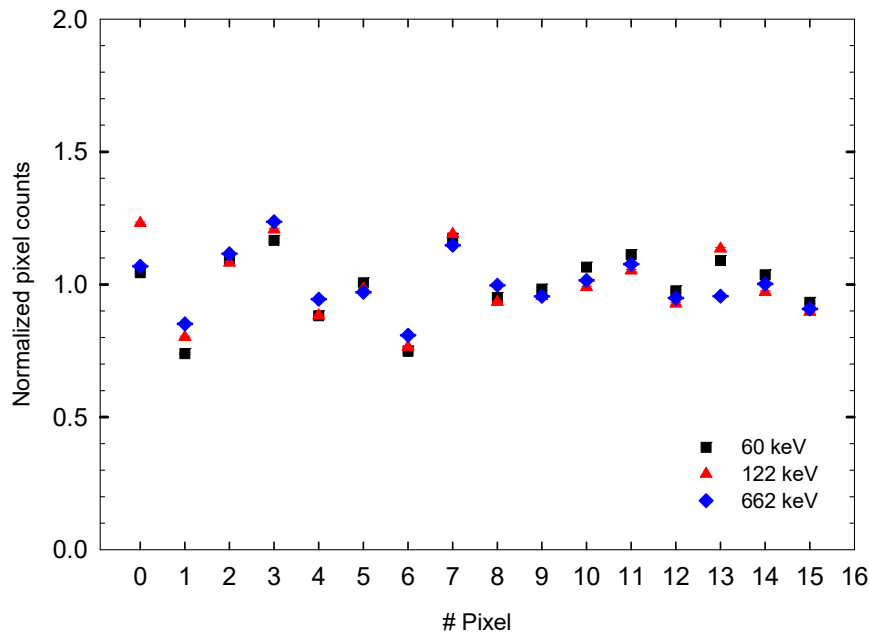


**Fig. 14a.** Behaviour of the *normalized counts* and the *normalized photopeak area* for 698300.

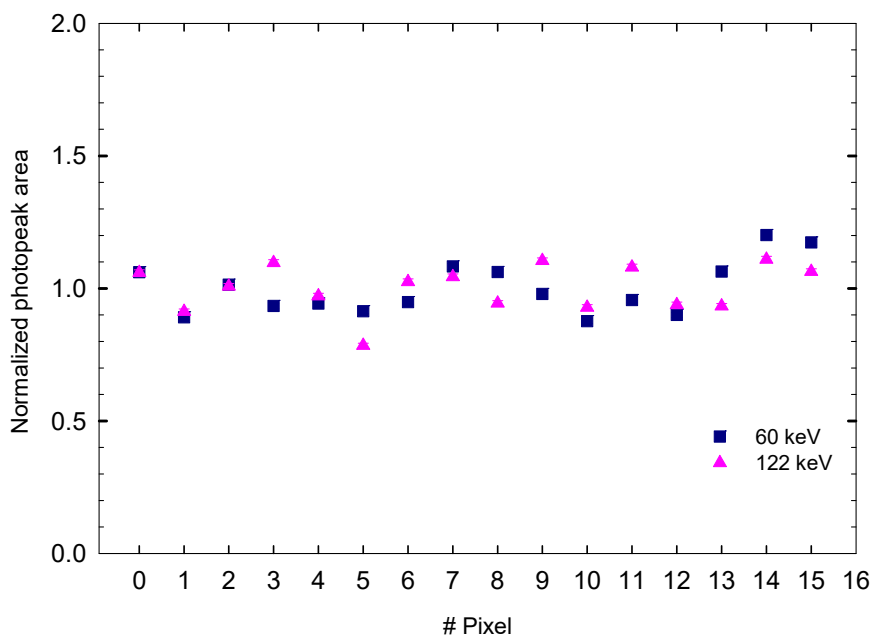
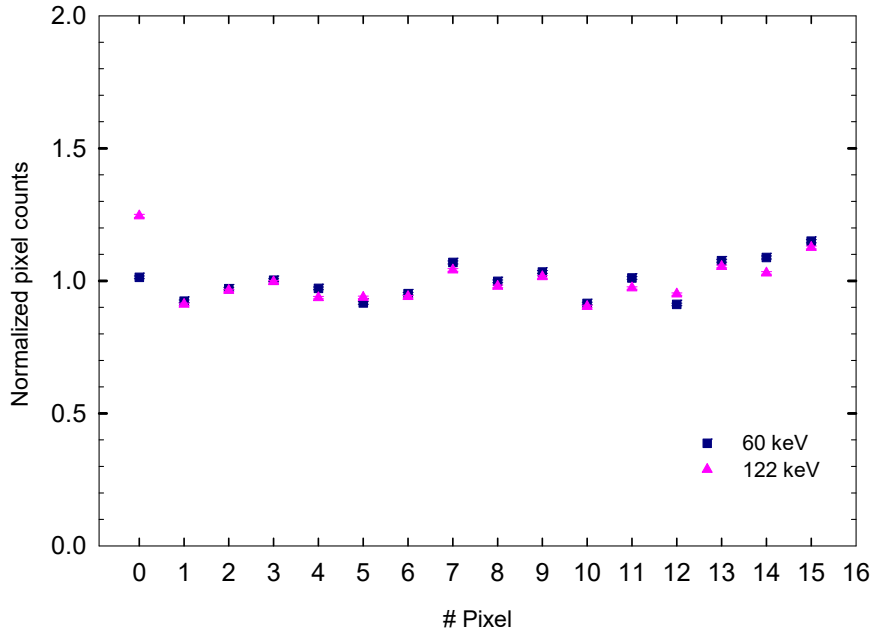


**Fig. 14b.** Behaviour of the *normalized counts* and the *normalized photopeak area* for P51134.

The maximum dispersion of two parameters defined above is about 30% at 14 keV, ~15% at 60, 122 and 662 keV for detector 698300 and about 10% for P51134.

#### 4.5. Energy Threshold

The measurements carried out confirm the ASIC specifications about energy threshold, which is <10 keV, ~8 keV.

#### 4.6. Stability of P51134 detector

The term polarization is used to refer to any change in the performance of a detector over time. We observed a polarization effect in the CdTe detectors during room temperature operation, that determines a decrease of the electric field effective in the detector volume, mainly due to the space charge created at the deep trapping sites. Consequently the drift velocity of charge carriers reduces and the charge collection times lengthens, increasing the trapping probability. This causes the degradation of the pulse height and shape with run time on continuous operation.

This figure shows a sequence of  $^{57}\text{Co}$  spectra acquired over a one-week period after applying 512 V. We can observe that there is not a significant variation in FWHM as in the peak position and amplitude.

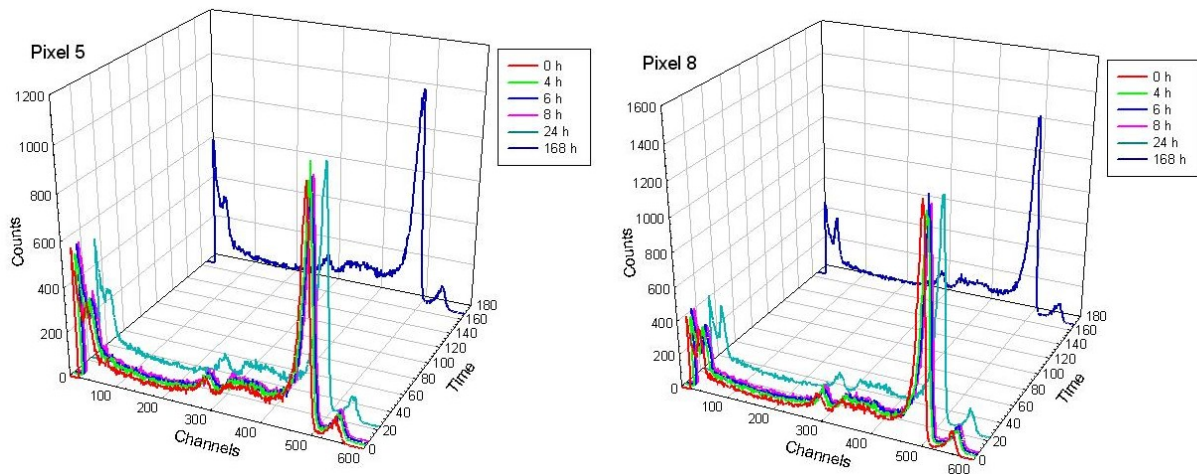


**Fig. 16.** Plot of  $^{57}\text{Co}$  spectra acquired over a 7 days period from P51134 detector. The pixel 8 presents the better energy resolution, while the pixel 5 is noisy at low energy.

An alternative approach to determine the stability of a detector is based upon the evaluation of the ratio named Quality Factor:

$$Q.F. = \frac{P/V}{\%FWHM}$$

As is shown in fig. 15, the detector used is stable over time.

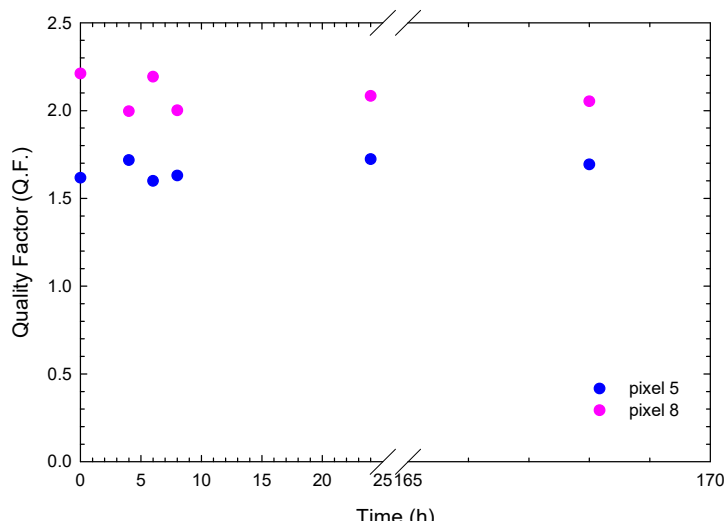


**Fig. 15.** Stability of CZT pixels as a function of the time.

<b>IASF- Sez. di Bologna</b>	<b>SCIENTIFIC PERFORMANCE REPORT</b>	<i>Ref:R P Issue: 1 Date: 03/02/04 page: 29/41</i>
--------------------------------------	--------------------------------------	--

After about 2 month of continuous operation without irradiating the detector, we have noted that the every pixel peak position is increased; we suggest that detrapped charge carriers from levels in the crystal are responsible for this effect.

### **5. Conclusions**

The results of the functional tests are:

- only the ASIC channel 0 is noisy;
- the energy threshold is ~8 keV.

Both tested detectors show very good performances:

- the uniformity of the photopeak position (gain) is about 1%;
- the energy resolution is ~4.9 % at 60 keV, ~2.9 % at 122 keV and 1.5 % at 662 keV;
- the uniformity of the energy resolution ( $\Delta E/E$ ) is about 10 % at 60 keV and 8 % at 122 keV;
- the uniformity of the *normalized counts* and *normalized photopeak area* ranges between 10 - 15% at 60, 122 keV for detector 698300 and about 10% for P51134.

<b>IASF- Sez. di Bologna</b>	<b>SCIENTIFIC PERFORMANCE REPORT</b>	<i>Ref: R P Issue: 1 Date: 03/02/04 page: 30/41</i>
--------------------------------------	--------------------------------------	---

### **Annex 1 Measurement Logbook**

Version of the logbook of the Multipixel detector calibration measurements performed at IASF-Sez. Bologna in January 2004. The last two numbers of file name represents the irradiated pixel number.

File	Gain	S.T. μs	Live Time s	LLD	Note
<b>gain 200\PT 0.6</b>					
Co57-02.s0	200	0.6	450	5.24	Shaping time characterization, $^{57}\text{Co}$ n. 13, Pb Collimator, $\phi = 5$ mm
Co57-06.s0	200	0.6	450	5.24	Shaping time characterization, $^{57}\text{Co}$ n. 13, Pb Collimator, $\phi = 5$ mm
Co57-11.s0	200	0.6	450	5.24	Shaping time characterization, $^{57}\text{Co}$ n. 13, Pb Collimator, $\phi = 5$ mm
Co57-15.s0	200	0.6	200	5.24	Shaping time characterization, $^{57}\text{Co}$ n. 13, Pb Collimator, $\phi = 5$ mm
Co57-15.s0	200	0.6	450	5.24	Shaping time characterization, $^{57}\text{Co}$ n. 13, Pb Collimator, $\phi = 5$ mm
<b>gain 200\PT 2.4</b>					
Co57-02.s0	200	2.4	230	5.24	Shaping time characterization, $^{57}\text{Co}$ n. 13, Pb Collimator, $\phi = 5$ mm
Co57-06.s0	200	2.4	200	5.24	Shaping time characterization, $^{57}\text{Co}$ n. 13, Pb Collimator, $\phi = 5$ mm
Co57-11.s0	200	2.4	200	5.24	Shaping time characterization, $^{57}\text{Co}$ n. 13, Pb Collimator, $\phi = 5$ mm
Co57-15.s0	200	2.4	200	5.24	Shaping time characterization, $^{57}\text{Co}$ n. 13, Pb Collimator, $\phi = 5$ mm
Co57-02.s0	200	2.4	200	5.24	Shaping time characterization, $^{57}\text{Co}$ n. 13, Pb Collimator, $\phi = 5$ mm
<b>gain 200\PT 1.2</b>					
Co57-00.s0	200	1.2	200	5.24	Spectrum, $^{57}\text{Co}$ n. 13, Pb Collimator, $\phi = 5$ mm
Co57-01.s0	200	1.2	200	5.24	Spectrum, $^{57}\text{Co}$ n. 13, Pb Collimator, $\phi = 5$ mm
Co57-02.s0	200	1.2	200	5.24	Spectrum, $^{57}\text{Co}$ n. 13, Pb Collimator, $\phi = 5$ mm
Co57-03.s0	200	1.2	200	5.24	Spectrum, $^{57}\text{Co}$ n. 13, Pb Collimator, $\phi = 5$ mm
Co57-04.s0	200	1.2	200	5.24	Spectrum, $^{57}\text{Co}$ n. 13, Pb Collimator, $\phi = 5$ mm
Co57-05.s0	200	1.2	200	5.24	Spectrum, $^{57}\text{Co}$ n. 13, Pb Collimator, $\phi = 5$ mm
Co57-06.s0	200	1.2	200	5.24	Spectrum, $^{57}\text{Co}$ n. 13, Pb Collimator, $\phi = 5$ mm
Co57-07.s0	200	1.2	200	5.24	Spectrum, $^{57}\text{Co}$ n. 13, Pb Collimator, $\phi = 5$ mm
Co57-08.s0	200	1.2	200	5.24	Spectrum, $^{57}\text{Co}$ n. 13, Pb Collimator, $\phi = 5$ mm
Co57-09.s0	200	1.2	200	5.24	Spectrum, $^{57}\text{Co}$ n. 13, Pb Collimator, $\phi = 5$ mm
Co57-10.s0	200	1.2	200	5.24	Spectrum, $^{57}\text{Co}$ n. 13, Pb Collimator, $\phi = 5$ mm
Co57-11.s0	200	1.2	200	5.24	Spectrum, $^{57}\text{Co}$ n. 13, Pb Collimator, $\phi = 5$ mm
Co57-12.s0	200	1.2	200	5.24	Spectrum, $^{57}\text{Co}$ n. 13, Pb Collimator, $\phi = 5$ mm
Co57-13.s0	200	1.2	200	5.24	Spectrum, $^{57}\text{Co}$ n. 13, Pb Collimator, $\phi = 5$ mm
Co57-14.s0	200	1.2	200	5.24	Spectrum, $^{57}\text{Co}$ n. 13, Pb Collimator, $\phi = 5$ mm
Co57-15.s0	200	1.2	200	5.24	Spectrum, $^{57}\text{Co}$ n. 13, Pb Collimator, $\phi = 5$ mm
Co57-15st.s0	200	1.2	200	5.24	Spectrum, $^{57}\text{Co}$ n. 13, Pb Collimator, $\phi = 5$ mm
<b>gain 100\PT 0.6</b>					
Co57-02.s0	100	0.6	200	5.24	Shaping time characterization, $^{57}\text{Co}$ n. 13, Pb Collimator, $\phi = 5$ mm
Co57-06.s0	100	0.6	200	5.24	Shaping time characterization, $^{57}\text{Co}$ n. 13, Pb Collimator, $\phi = 5$ mm
Co57-11.s0	100	0.6	200	5.24	Shaping time characterization, $^{57}\text{Co}$ n. 13, Pb Collimator, $\phi = 5$ mm
Co57-15.s0	100	0.6	200	5.24	Shaping time characterization, $^{57}\text{Co}$ n. 13, Pb Collimator, $\phi = 5$ mm
<b>gain 100\PT 2.4</b>					
Co57-02.s0	100	2.4	200	5.24	Shaping time characterization, $^{57}\text{Co}$ n. 13, Pb Collimator, $\phi = 5$ mm
Co57-06.s0	100	2.4	200	5.24	Shaping time characterization, $^{57}\text{Co}$ n. 13, Pb Collimator, $\phi = 5$ mm
Co57-11.s0	100	2.4	200	5.24	Shaping time characterization, $^{57}\text{Co}$ n. 13, Pb Collimator, $\phi = 5$ mm
Co57-15.s0	100	2.4	200	5.24	Shaping time characterization, $^{57}\text{Co}$ n. 13, Pb Collimator, $\phi = 5$ mm
<b>gain 100\PT 1.2</b>					
Co57-00.s0	100	1.2	200	5.24	Spectrum, $^{57}\text{Co}$ n. 13, Pb Collimator, $\phi = 5$ mm
Co57-01.s0	100	1.2	200	5.24	Spectrum, $^{57}\text{Co}$ n. 13, Pb Collimator, $\phi = 5$ mm
Co57-02.s0	100	1.2	200	5.24	Spectrum, $^{57}\text{Co}$ n. 13, Pb Collimator, $\phi = 5$ mm
Co57-03.s0	100	1.2	200	5.24	Spectrum, $^{57}\text{Co}$ n. 13, Pb Collimator, $\phi = 5$ mm
Co57-04.s0	100	1.2	200	5.24	Spectrum, $^{57}\text{Co}$ n. 13, Pb Collimator, $\phi = 5$ mm
Co57-05.s0	100	1.2	200	5.24	Spectrum, $^{57}\text{Co}$ n. 13, Pb Collimator, $\phi = 5$ mm
Co57-06.s0	100	1.2	200	5.24	Spectrum, $^{57}\text{Co}$ n. 13, Pb Collimator, $\phi = 5$ mm
Co57-07.s0	100	1.2	200	5.24	Spectrum, $^{57}\text{Co}$ n. 13, Pb Collimator, $\phi = 5$ mm
Co57-08.s0	100	1.2	200	5.24	Spectrum, $^{57}\text{Co}$ n. 13, Pb Collimator, $\phi = 5$ mm
Co57-09.s0	100	1.2	200	5.24	Spectrum, $^{57}\text{Co}$ n. 13, Pb Collimator, $\phi = 5$ mm
Co57-10.s0	100	1.2	200	5.24	Spectrum, $^{57}\text{Co}$ n. 13, Pb Collimator, $\phi = 5$ mm
Co57-11.s0	100	1.2	200	5.24	Spectrum, $^{57}\text{Co}$ n. 13, Pb Collimator, $\phi = 5$ mm
Co57-12.s0	100	1.2	200	5.24	Spectrum, $^{57}\text{Co}$ n. 13, Pb Collimator, $\phi = 5$ mm
Co57-13.s0	100	1.2	200	5.24	Spectrum, $^{57}\text{Co}$ n. 13, Pb Collimator, $\phi = 5$ mm
Co57-14.s0	100	1.2	200	5.24	Spectrum, $^{57}\text{Co}$ n. 13, Pb Collimator, $\phi = 5$ mm

<i><b>IASF- Sez. di Bologna</b></i>	<b>SCIENTIFIC PERFORMANCE REPORT</b>	<i>Ref: R P Issue: 1 Date: 03/02/04 page: 31/41</i>
---	--------------------------------------	---

<b>IASF- Sez. di Bologna</b>	<b>SCIENTIFIC PERFORMANCE REPORT</b>					<i>Ref:R P Issue: 1 Date: 03/02/04 page: 32/41</i>
--------------------------------------	--------------------------------------	--	--	--	--	--

Co57-07.s0	50	1.2	30	5.24	Spectrum, $^{57}\text{Co}$ n. 13, Pb Collimator, $\phi = 3.5$ mm	
Co57-08.s0	50	1.2	30	5.24	Spectrum, $^{57}\text{Co}$ n. 13, Pb Collimator, $\phi = 3.5$ mm	
Co57-09.s0	50	1.2	30	5.24	Spectrum, $^{57}\text{Co}$ n. 13, Pb Collimator, $\phi = 3.5$ mm	
Co57-10.s0	50	1.2	30	5.24	Spectrum, $^{57}\text{Co}$ n. 13, Pb Collimator, $\phi = 3.5$ mm	
Co57-11.s0	50	1.2	30	5.24	Spectrum, $^{57}\text{Co}$ n. 13, Pb Collimator, $\phi = 3.5$ mm	
Co57-12.s0	50	1.2	30	5.24	Spectrum, $^{57}\text{Co}$ n. 13, Pb Collimator, $\phi = 3.5$ mm	
Co57-13.s0	50	1.2	30	5.24	Spectrum, $^{57}\text{Co}$ n. 13, Pb Collimator, $\phi = 3.5$ mm	
Co57-14.s0	50	1.2	30	5.24	Spectrum, $^{57}\text{Co}$ n. 13, Pb Collimator, $\phi = 3.5$ mm	
Co57-15.s0	50	1.2	30	5.24	Spectrum, $^{57}\text{Co}$ n. 13, Pb Collimator, $\phi = 3.5$ mm	
<b>gain 50\PT 1.2</b>						
Cs137-00.s0	50	1.2	2700	5.24	Spectrum, uncollimated $^{137}\text{Cs}$ n. 4	
Cs137-01.s0	50	1.2	2700	5.24	Spectrum, uncollimated $^{137}\text{Cs}$ n. 4	
Cs137-02.s0	50	1.2	2700	5.24	Spectrum, uncollimated $^{137}\text{Cs}$ n. 4	
Cs137-03.s0	50	1.2	2700	5.24	Spectrum, uncollimated $^{137}\text{Cs}$ n. 4	
Cs137-04.s0	50	1.2	2700	5.24	Spectrum, uncollimated $^{137}\text{Cs}$ n. 4	
Cs137-05.s0	50	1.2	2700	5.24	Spectrum, uncollimated $^{137}\text{Cs}$ n. 4	
Cs137-06.s0	50	1.2	2700	5.24	Spectrum, uncollimated $^{137}\text{Cs}$ n. 4	
Cs137-07.s0	50	1.2	2700	5.24	Spectrum, uncollimated $^{137}\text{Cs}$ n. 4	
Cs137-08.s0	50	1.2	2700	5.24	Spectrum, uncollimated $^{137}\text{Cs}$ n. 4	
Cs137-09.s0	50	1.2	2700	5.24	Spectrum, uncollimated $^{137}\text{Cs}$ n. 4	
Cs137-10.s0	50	1.2	2700	5.24	Spectrum, uncollimated $^{137}\text{Cs}$ n. 4	
Cs137-11.s0	50	1.2	2700	5.24	Spectrum, uncollimated $^{137}\text{Cs}$ n. 4	
Cs137-12.s0	50	1.2	2700	5.24	Spectrum, uncollimated $^{137}\text{Cs}$ n. 4	
Cs137-13.s0	50	1.2	2700	5.24	Spectrum, uncollimated $^{137}\text{Cs}$ n. 4	
Cs137-14.s0	50	1.2	2700	5.24	Spectrum, uncollimated $^{137}\text{Cs}$ n. 4	
Cs137-15.s0	50	1.2	2700	5.24	Spectrum, uncollimated $^{137}\text{Cs}$ n. 4	
Cs-00-5m.s0	50	1.2	2700	5.24	Spectrum, uncollimated $^{137}\text{Cs}$ n. 4	
<b>gain 50\PT 1.2</b>						
Co57-00.s0	50	1.2	20	5.24	Spectrum, uncollimated $^{57}\text{Co}$ n. 13	
Co57-01.s0	50	1.2	20	5.24	Spectrum, uncollimated $^{57}\text{Co}$ n. 13	
Co57-02.s0	50	1.2	20	5.24	Spectrum, uncollimated $^{57}\text{Co}$ n. 13	
Co57-03.s0	50	1.2	20	5.24	Spectrum, uncollimated $^{57}\text{Co}$ n. 13	
Co57-04.s0	50	1.2	20	5.24	Spectrum, uncollimated $^{57}\text{Co}$ n. 13	
Co57-05.s0	50	1.2	20	5.24	Spectrum, uncollimated $^{57}\text{Co}$ n. 13	
Co57-06.s0	50	1.2	20	5.24	Spectrum, uncollimated $^{57}\text{Co}$ n. 13	
Co57-07.s0	50	1.2	20	5.24	Spectrum, uncollimated $^{57}\text{Co}$ n. 13	
Co57-08.s0	50	1.2	20	5.24	Spectrum, uncollimated $^{57}\text{Co}$ n. 13	
Co57-09.s0	50	1.2	20	5.24	Spectrum, uncollimated $^{57}\text{Co}$ n. 13	
Co57-10.s0	50	1.2	20	5.24	Spectrum, uncollimated $^{57}\text{Co}$ n. 13	
Co57-11.s0	50	1.2	20	5.24	Spectrum, uncollimated $^{57}\text{Co}$ n. 13	
Co57-12.s0	50	1.2	20	5.24	Spectrum, uncollimated $^{57}\text{Co}$ n. 13	
Co57-13.s0	50	1.2	20	5.24	Spectrum, uncollimated $^{57}\text{Co}$ n. 13	
Co57-14.s0	50	1.2	20	5.24	Spectrum, uncollimated $^{57}\text{Co}$ n. 13	
Co57-15.s0	50	1.2	20	5.24	Spectrum, uncollimated $^{57}\text{Co}$ n. 13	
15fondo.s0	50	1.2	2700	5.24	Background spectrum of pixel 15	
<b>gain 33</b>						
Co-57-00	33	1.2	40	0.49	Spectrum, uncollimated $^{57}\text{Co}$ n. 13	
Co-57-02	33	1.2	40	0.49	Spectrum, uncollimated $^{57}\text{Co}$ n. 13	
Co-57-05	33	1.2	40	0.49	Spectrum, uncollimated $^{57}\text{Co}$ n. 13	
Co-57-06	33	1.2	40	0.49	Spectrum, uncollimated $^{57}\text{Co}$ n. 13	
Co-57-11	33	1.2	40	0.49	Spectrum, uncollimated $^{57}\text{Co}$ n. 13	
Co-57-15	33	1.2	40	0.49	Spectrum, uncollimated $^{57}\text{Co}$ n. 13	
Cs137-06	33	1.2	200	0.49	Spectrum, uncollimated $^{137}\text{Cs}$ n. 4	
Cs137-11	33	1.2	200	0.49	Spectrum, uncollimated $^{137}\text{Cs}$ n. 4	
<b>gain 200\no coll</b>						
Co57-00.s0	200	1.2	50	25.23	Spectrum, uncollimated $^{57}\text{Co}$ n. 13, Pb cover, low discriminator level	
Co57-00 .s0	200	1.2	50	25.23	Spectrum, uncollimated $^{57}\text{Co}$ n. 13, Pb cover	
Co002023.s0	200	1.2	50	20.23	Spectrum, uncollimated $^{57}\text{Co}$ n. 13, Pb cover	
Co57-01.s0	200	1.2	50	20.23	Spectrum, uncollimated $^{57}\text{Co}$ n. 13, Pb cover	
Co57-02.s0	200	1.2	50	20.23	Spectrum, uncollimated $^{57}\text{Co}$ n. 13, Pb cover	
Co57-03.s0	200	1.2	50	20.23	Spectrum, uncollimated $^{57}\text{Co}$ n. 13, Pb cover	
Co57-04.s0	200	1.2	50	20.23	Spectrum, uncollimated $^{57}\text{Co}$ n. 13, Pb cover	
Co57-05.s0	200	1.2	50	20.23	Spectrum, uncollimated $^{57}\text{Co}$ n. 13, Pb cover	
Co57-06.s0	200	1.2	50	20.23	Spectrum, uncollimated $^{57}\text{Co}$ n. 13, Pb cover	

<i>IASF- Sez. di Bologna</i>	<b>SCIENTIFIC PERFORMANCE REPORT</b>	<i>Ref: R P Issue: 1 Date: 03/02/04 page: 33/41</i>
--------------------------------------	--------------------------------------	---

*Annex 2 Fitting models*  
 **$^{57}\text{Co}$  radioactive source: 122 keV line**

